# Saikosaponin D overcomes gemcitabine resistance in pancreatic cancer via AKT/mTOR pathway inhibition and synergistic induction of apoptosis and autophagy

RUI ZHENG[1*], YUSI LIU[1*], SEN ZHOU[1], GUIMEI LIU[2], XIAOBIN LIU[1], YIYUAN YANG[1] and YUFU ZHANG[3]

[1]Department of Medical Immunology, Yan'an Medical College, Yan'an University, Yan'an, Shaanxi 716000, P.R. China;
[2]Department of Clinical Laboratory, The Affiliated Hospital of Yan'an University, Yan'an, Shaanxi 716000, P.R. China;
[3]Department of Hepatobiliary and Pancreatic Surgery, The Affiliated Hospital of Yan'an University, Yan'an, Shaanxi 716000, P.R. China

Received June 9, 2025; Accepted September 8, 2025

DOI: 10.3892/or.2025.9033

**Abstract.** Gemcitabine (GEM) is the first-line chemotherapy drug for pancreatic cancer, but its efficacy is often limited by inherent drug resistance. Saikosaponin D (SSD), a bioactive triterpenoid saponin derived from the *Bupleurum chinense* root, exhibits anti-inflammatory and antitumor properties; however, to the best of our knowledge, its role in pancreatic cancer and GEM sensitization remains unclear. The present study investigated the effects of SSD on the proliferation, apoptosis and autophagy of pancreatic cancer cells, and evaluated whether SSD can overcome GEM resistance to enhance its antitumor effects. Using MIA PaCa-2 and AsPC-1 cells, the sensitivity to SSD and GEM was assessed using Cell Counting Kit-8 assays, H&E staining and colony formation assays. Optimal sub-lethal concentrations of GEM (0.25 $\mu$mol/l), SSD (4 $\mu$mol/l) and their combination (0.25 $\mu$mol/l GEM + 4 $\mu$mol/l SSD) were identified. Apoptosis was evaluated through Hoechst 33258 staining and TUNEL assays, while autophagy was measured using the monodasylcadaverine method. Western blotting and immunocytochemical staining were used to analyze the expression levels of proteins related to apoptosis, AKT/mTOR signaling and autophagy. The results demonstrated that the SSD + GEM combination significantly inhibited pancreatic cancer cell proliferation in both MIA PaCa-2 and AsPC-1 cell lines, with proliferation being suppressed by nearly half. Similarly, the combination treatment induced apoptosis and enhanced autophagosome formation, suggesting potential synergistic effects when compared with GEM monotherapy. In conclusion, SSD synergistically enhanced the antitumor effects of GEM by inhibiting pancreatic cancer cell proliferation, and inducing apoptosis and autophagy. SSD may overcome GEM resistance by sensitizing cells through AKT/mTOR pathway inhibition.

*Correspondence to:* Dr Yufu Zhang, Department of Hepatobiliary and Pancreatic Surgery, The Affiliated Hospital of Yan'an University, 43 North Street, Baota, Yan'an, Shaanxi 716000, P.R. China
E-mail: zyf890908@163.com

*Contributed equally

*Key words:* gemcitabine, Saikosaponin D, pancreatic cancer, apoptosis, autophagy, AKT/mTOR signaling pathway

## Introduction

Pancreatic cancer is a highly lethal malignant tumor. Due to the lack of specific symptoms in its early stage and its highly aggressive nature, patients are usually diagnosed at later stages of the disease (1,2). Therefore, the prognosis for pancreatic cancer is poor, with 5-year survival rates of ≤10% (3). Despite major advances in oncology in recent years, the treatment of pancreatic cancer remains a challenge. Currently, the main clinical treatment methods include surgery, radiotherapy and chemotherapy, with surgery remaining the most effective option. However, only 15-20% of patients qualify for surgical treatment, and even after surgery, recurrence and metastasis remain highly prevalent (4). Gemcitabine (GEM) is a deoxycytidine analog that inhibits DNA replication and is widely used for the treatment of various cancer types, including pancreatic, non-small cell lung, bladder, ovarian and breast cancer (5,6). For patients with inoperable locally advanced and metastatic pancreatic cancer, GEM monotherapy or GEM-based combination chemotherapy remain first-line choices (7). However, enzymatic deamination, rapid systemic clearance and the emergence of chemoresistance all limit GEM efficacy, favoring recurrence and metastasis (6). Therefore, exploring the mechanisms underlying GEM resistance, improving the sensitivity of pancreatic cancer cells to GEM and identifying novel targeted therapeutic drugs is paramount.

The AKT/mTOR signaling pathway crucially influences basic cellular processes such as protein synthesis, and cell growth, proliferation and metabolism, and also participates in the regulation of autophagy, apoptosis and angiogenesis (8,9). Over-activation of the AKT/mTOR signaling pathway has been reported in various tumors, such as skin cancer (10), breast cancer (11), thyroid cancer (12), non-small cell lung cancer (NSCLC) (13) and prostate cancer (14). Abnormal activation of this pathway is also closely related to the occurrence and development of pancreatic cancer (15). Furthermore, sustained

activation of AKT/mTOR signaling enhances drug resistance in pancreatic cancer cells, and creates favorable conditions for their survival and proliferation by enhancing metabolic activity and inhibiting apoptosis (16). Therefore, therapeutic inhibition of the AKT/mTOR pathway has become an important goal in the treatment of pancreatic cancer.

At present, strategies for reversing drug resistance in tumor cells mainly include the following approaches: Targeted inhibition of drug resistance pathways, combination treatments with conventional agents, administration of traditional Chinese medicine (TCM) prescriptions, nano-drug delivery systems and gene editing (17,18). Among these, TCM compounds are particularly notable for their ability to regulate multiple targets. This multi-target action can not only enhance the efficacy of anticancer drugs but also reduce their associated cytotoxicity and other side effects (19). Bupleurum, also known as Radix Bupleuri or 'Chai Hu', is a classical herb within TCM (20). Saikosaponin D (SSD), one of the major bioactive ingredients of Bupleurum, possesses anti-inflammatory, antioxidant and immunoregulatory properties (20). Our previous study demonstrated that SSD exerted cytotoxic effects on glioma cells and enhanced their sensitivity to temozolomide chemotherapy (21). Previous research has further demonstrated that SSD has growth inhibitory and pro-apoptotic effects in a variety of solid tumors. For example, Tang *et al* (22) found that SSD enhanced the sensitivity of human NSCLC cells to gefitinib by inhibiting STAT3/Bcl-2 signaling, thereby inducing tumor cell apoptosis. Hu *et al* (23) demonstrated that SSD enhanced the sensitivity of human gastric cancer cells to cisplatin by inhibiting the IKKβ/NF-κB pathway. In addition, Zhang *et al* (24) found that SSD suppressed the malignant phenotype of Hep3B hepatoma cells and increased the sensitivity of these cells to chemotherapy *in vitro* and *in vivo*. However, studies on the combination of SSD and GEM in pancreatic cancer remain scarce. Thus, it remains unclear whether SSD can enhance the sensitivity of pancreatic cancer cells to GEM and effectively overcome GEM resistance. Furthermore, although the antitumor activity of SSD has been extensively studied in multiple solid tumors, where they demonstrated strong potential for apoptosis induction through multiple pathways (25,26), it is not clear whether combined administration of SSD and chemotherapy agents induces apoptosis via regulation of the AKT/mTOR pathway. In addition, to the best of our knowledge, it remains unknown whether SSD can improve the chemosensitivity of pancreatic cancer cells to GEM by downregulating AKT/mTOR signaling. Therefore, the present study aimed to investigate whether SSD could enhance the sensitivity to GEM chemotherapy, regulate AKT/mTOR activation, and promote apoptosis and autophagy in pancreatic cancer cells.

## Materials and methods

*Reagents and antibodies*. SSD (purity ≥98% as determined by high-performance liquid chromatography) was obtained from Shanghai Yuanye Biotechnology Co., Ltd. GEM was purchased from GLPBIO Technology LLC. Stock solutions of each drug (1 mmol/l) were prepared by dissolution in DMSO and stored protected from light at -20˚C. The Cell Counting Kit-8 (CCK-8), Hoechst 33258 staining kit and immunocytochemistry (ICC) staining kit were acquired from Wuhan Boster Biological Technology Co., Ltd. The Autophagy Dual Stain kit [using monodansylcadaverine (MDC)] and 0.1% crystal violet ammonium oxalate solution were procured from Beijing Solarbio Science & Technology Co., Ltd. The BCA protein assay kit was obtained from the Beyotime Institute of Biotechnology. The TUNEL Apoptosis Assay kit was purchased from TransGen Biotech Co., Ltd. The following antibodies were purchased from Proteintech Group, Inc.: Mouse monoclonal antibodies against mTOR (1:500; cat. no. 66888-1-Ig), phosphorylated (p-)mTOR (Ser2448) (1:2,000; cat. no. 67778-1-Ig), p-AKT (Ser473) (1:500; cat. no. 66444-1-Ig), caspase-3 (1:2,000; cat. no. 66470-2-Ig), cleaved caspase-3 (1:1,000; cat. no. 66470-2-Ig), Bax (1:500; cat. no. 60267-1-Ig), AKT (1:500; cat. no. 60203-2-Ig) and β-actin (1:2,000; cat. no. 66009-1-Ig); as well as rabbit antibodies, including polyclonal antibodies against Bcl-2 (1:1,000; cat. no. 12789-1-AP), Beclin 1 (1:1,000; cat. no. 11306-1-AP) and LC3 (1:1,000; cat. no. 14600-1-AP). The same monoclonal antibody (cat. no. 66470-2-Ig) was used for the detection of both total caspase-3 (at 1:2,000 dilution) and cleaved caspase-3 (at 1:1,000 dilution), as it recognizes an epitope shared by both forms of the protein. The higher antibody concentration (1:1,000) for cleaved caspase-3 was used due to its lower abundance post-cleavage, ensuring optimal detection sensitivity. Additionally, a separate rabbit monoclonal anti-Bax antibody (1:1,000; cat. no. 5023T) was obtained from Cell Signaling Technology, Inc., for western blotting. Peroxidase-conjugated anti-mouse (1:5,000; cat. no. SA00001-1) and anti-rabbit (1:5,000; cat. no. SA00001-2) secondary antibodies were also obtained from Proteintech Group, Inc.

*Chemical structure illustration*. The chemical structures of SSD and GEM were generated based on their canonical representations from the PubChem database (National Center for Biotechnology Information; https://pubchem.ncbi.nlm.nih.gov/), using their unique Compound Identifiers (119361 for SSD and 60750 for GEM), and were subsequently exported in high-resolution TIFF format for publication.

*Cell lines and culture*. The MIA PaCa-2 and AsPC-1 human pancreatic adenocarcinoma cell lines were obtained from the cell bank of the Yan'an University Medical Research and Experimental Center (Yan'an, China). The MIA PaCa-2 and AsPC-1 cell lines were originally acquired from American Type Culture Collection. MIA PaCa-2 and AsPC-1 cells were cultured in DMEM (cat. no. 11965092; Gibco; Thermo Fisher Scientific, Inc.) and RPMI-1640 medium (cat. no. 11875093; Gibco; Thermo Fisher Scientific, Inc.), respectively, supplemented with 10% FBS (cat. no. 10270106; Gibco; Thermo Fisher Scientific, Inc.) and 1% penicillin-streptomycin (cat. no. 15140122; Gibco; Thermo Fisher Scientific, Inc.). Both cell lines were maintained at 37˚C in a 5% $CO_2$ humidified incubator. Cells in the logarithmic growth phase were plated for downstream experiments.

*Cell viability assay*. MIA PaCa-2 and AsPC-1 cell suspensions were prepared, and cells were seeded into 96-well cell culture plates (100 $\mu$l; 2.5x$10^3$ cells/well), and treated with SSD (0, 2, 4, 6, 8, 10 or 12 $\mu$mol/l) or GEM (0, 0.25, 0.5, 1, 2, 4 or 8 $\mu$mol/l) for 24, 48 or 72 h at 37˚C. CCK-8 reagent was

added to each well and cells were incubated in the dark for 1 h at 37˚C. Absorbance values were subsequently measured at 450 nm using a microplate reader. Cell viability was calculated using GraphPad Prism 9 software (Dotmatics). According to the effects of SSD and GEM and their respective $IC_{50}$, a GEM dose of 0.25 $\mu$mol/l (referred to as G0.25) and SSD doses of 4 or 6 $\mu$mol/l (referred to as S4 and S6, respectively) were selected for downstream assays to treat MIA PaCa-2 and AsPC-1 cells. Control groups were treated with an equal volume of the drug solvent (DMSO) alone, with the final DMSO concentration not exceeding 0.1% in all groups.

*Synergy analysis*. Drug interaction effects were quantitatively analyzed using the Chou-Talalay method (27). Combination Index (CI) values were calculated from dose-effect curves generated based on CCK-8 and TUNEL assays, where a CI of <1, =1 and >1 indicates synergy, additive effects and antagonism, respectively. CalcuSyn software (version 2.0; Biosoft) was employed for CI calculation with the following parameters: Fraction affected range, 0.05-0.95; and median-effect principle for dose-effect relationship modeling.

*Cell morphology evaluation*. Cell morphology and structure were evaluated by H&E staining, whereby MIA PaCa-2 and AsPC-1 cells were seeded onto sterile glass coverslips in 6-well plates at a density of $5x10^4$ cells/well, allowed to adhere overnight, and treated with a range of concentrations of SSD (0-12 $\mu$mol/l), GEM (0-8 $\mu$mol/l) or the combination of G0.25 + S4 for 48 h at 37˚C. After treatment, all subsequent steps were performed at room temperature. Briefly, cells were washed with PBS, fixed in 95% ethanol for 20 min, and stained with Harris's hematoxylin (cat. no. HHS32; Sigma-Aldrich; Merck KGaA) for 8 min. This was followed by differentiation in 1% acid alcohol for 30 sec, bluing in 0.2% ammonia water and counterstaining with eosin Y (cat. no. HT110232; Sigma-Aldrich; Merck KGaA) for 3 min. The samples were then dehydrated through an ascending graded ethanol series, cleared in xylene and mounted with neutral balsam. Morphology was evaluated under a light microscope (Nikon Eclipse Ti2; Nikon Corporation) by two independent observers. The vehicle control group (0.1% DMSO) was processed in parallel under identical conditions.

*Cell clone formation assay*. The cell clone formation assay was performed by seeding MIA PaCa-2 and AsPC-1 cells into 6-well plates at a density of $2x10^3$ cells/well, allowing them to adhere for 24 h at 37˚C in complete growth medium without treatment, after which the medium was replaced with fresh medium containing specified treatments [GEM (0.25 $\mu$mol/l), SSD (4 $\mu$mol/l), the combination G0.25 + S4, or vehicle control (0.1% DMSO)] and cells were cultured for 7-10 days at 37˚C with the medium being refreshed every 3 days. After incubation, the cells were washed with PBS, fixed with 4% paraformaldehyde (PFA) for 20 min at room temperature and stained with 0.1% crystal violet for 20 min at room temperature. The plates were then gently rinsed with distilled water to remove excess dye, air-dried and imaged using a light microscope. Colonies, defined as groups of ≥50 cells, were quantified using ImageJ software (version 1.53t; National Institutes of Health) by measuring the crystal violet-stained area after applying a consistent threshold. Results were expressed as a percentage of the control group.

*Hoechst 33258 staining*. Hoechst 33258 staining was performed by seeding MIA PaCa-2 and AsPC-1 cells on sterile glass coverslips in 6-well plates at a density of $5x10^4$ cells/well, allowing adhesion for 24 h at 37˚C in untreated complete medium, and then treating cells with GEM (0.25 $\mu$mol/l), SSD (4 $\mu$mol/l), G0.25 + S4 or vehicle (0.1% DMSO) for 48 h at 37˚C. After treatment, cells were fixed in 4% PFA for 20 min at room temperature, washed with PBS and then stained with Hoechst 33258 (5 $\mu$g/ml) for 5 min in the dark at room temperature. Following another wash with PBS, cells were mounted with anti-fade medium and imaged using a Nikon Eclipse Ti2 fluorescence microscope (Nikon Corporation) equipped with a DS-Qi2 camera (Nikon Corporation). Image analysis was conducted using NIS-Elements software (v5.30; Nikon Corporation).

*Autophagy assay*. The autophagy assay was performed by seeding MIA PaCa-2 and AsPC-1 cells into 12-well plates at a density of $5x10^4$ cells/well, followed by treatment the next day with GEM (0.25 $\mu$mol/l), SSD (4 $\mu$mol/l), their combination (G0.25 + S4) or vehicle control (0.1% DMSO) for 48 h at 37˚C in a 5% $CO_2$ humidified incubator. Subsequently, cells were processed using the Autophagy Dual Stain kit (MDC) (Beijing Solarbio Science & Technology Co., Ltd.) according to the manufacturer's instructions. Briefly, cells were washed with 1X PBS and fixed with the kit-provided fixative (4% paraformaldehyde; 20 min at 25˚C). After three washes with the kit-supplied 1X wash buffer, cells were incubated with the MDC working solution (200 $\mu$l/well; 60 min at 37˚C in the dark). Following three additional washes with 1X wash buffer, fresh 1X PBS was added to prevent drying. Image acquisition was performed immediately using a Nikon Eclipse Ti2 fluorescence microscope (Nikon Corporation) equipped with a DS-Qi2 camera. Quantitative analysis of fluorescence intensity was conducted using NIS-Elements software (v5.30; Nikon Corporation). Untreated control cells (0.1% DMSO) were processed in parallel under identical conditions.

*TUNEL*. The TUNEL assay was conducted by seeding MIA PaCa-2 and AsPC-1 cells onto coverslips in 24-well plates and allowing them to reach 70% confluence. Cells were then treated with 0.25 $\mu$mol/l GEM, 4 $\mu$mol/l SSD, their combination G0.25 + S4 or vehicle control (0.1% DMSO) for 48 h at 37˚C with 5% $CO_2$. After treatment, cells were washed three times with PBS and fixed with 4% PFA for 20 min at room temperature. Permeabilization was performed using 0.1% Triton X-100 for 5 min at room temperature. The TUNEL reaction mixture containing terminal deoxynucleotidyl transferase was applied to each sample, followed by incubation in a humidified dark chamber at 37˚C for 1 h. Subsequently, cells were washed with PBS and counterstained with DAPI at a concentration of 1 $\mu$g/ml for 10 min at room temperature. After a final rinse with PBS, coverslips were mounted using antifade mounting medium. Images from at least five random fields per coverslip were captured using a fluorescence microscope. Each assay included both a negative control without terminal transferase enzyme and a vehicle-treated DMSO control.

*Western blotting*. MIA PaCa-2 and AsPC-1 cells in the logarithmic growth phase were treated with 0.25 $\mu$mol/l GEM, 4 $\mu$mol/l SSD, their combination G0.25 + S4 or vehicle control (0.1% DMSO) for 48 h at 37˚C. Immediately following treatment, cells were harvested using EDTA-free trypsin, washed twice with cold phosphate-buffered saline, resuspended in precooled PBS and centrifuged at 1,000 x g for 5 min at 4˚C. The cell pellets were lysed on ice for 40 min using RIPA lysis buffer (P0013B; Beyotime Institute of Biotechnology) supplemented with 1% protease inhibitor cocktail (P1005; Beyotime Institute of Biotechnology). The lysates were centrifuged at 16,020 x g for 20 min at 4˚C, and the supernatant protein concentrations were determined using a BCA assay (P0010; Beyotime Institute of Biotechnology,). Equal amounts of protein (30 $\mu$g per lane) were separated on 10-15% SDS-polyacrylamide gels and transferred onto PVDF membranes. After blocking with 5% skim milk for 2 h at room temperature, the membranes were incubated overnight at 4˚C with the following primary antibodies: Mouse monoclonal anti-mTOR (1:500; cat. no. 66888-1-Ig; Proteintech Group, Inc.), anti-p-mTOR (Ser2448) (1:2,000; cat. no. 67778-1-Ig; Proteintech Group, Inc.), anti-p-AKT (Ser473) (1:500; cat. no. 66444-1-Ig; Proteintech Group, Inc.), anti-caspase-3 (1:2,000; cat. no. 66470-2-Ig; Proteintech Group, Inc.), anti-cleaved caspase-3 (1:1,000; cat. no. 66470-2-Ig; Proteintech Group, Inc.), anti-AKT (1:500; cat. no. 60203-2-Ig; Proteintech Group, Inc.) and anti-β-actin (1:2,000; cat. no. 66009-1-Ig; Proteintech Group, Inc.); and rabbit polyclonal anti-Bcl-2 (1:1,000; cat. no. 12789-1-AP; Proteintech Group, Inc.), anti-Beclin 1 (1:1,000; cat. no. 11306-1-AP; Proteintech Group, Inc.) and anti-LC3 (1:1,000; cat. no. 14600-1-AP; Proteintech Group, Inc.) antibodies, as well as an anti-Bax monoclonal antibody (1:1,000; cat. no. 5023T; Cell Signaling Technology, Inc.). The same monoclonal antibody (cat. no. 66470-2-Ig) was used for the detection of both total caspase-3 (at 1:2,000 dilution) and cleaved caspase-3 (at 1:1,000 dilution), as it recognizes an epitope shared by both forms of the protein. The higher antibody concentration (1:1,000) for cleaved caspase-3 was used due to its lower abundance post-cleavage, ensuring optimal detection sensitivity. The membranes were then washed three times with TBS with 0.1% Tween-20 (TBST) and incubated for 1.5 h at room temperature with HRP-conjugated goat anti-mouse (1:5,000; SA00001-1; Proteintech Group, Inc.) or goat anti-rabbit (1:5,000; SA00001-2; Proteintech Group, Inc.) secondary antibodies. Following three additional washes with TBST, the protein bands were visualized using an Enhanced Chemiluminescence reagent (P0018FS; Beyotime Institute of Biotechnology) and images were captured with a Bio-Rad ChemiDoc imaging system (Bio-Rad Laboratories, Inc.). Semi-quantitative analysis was performed using ImageJ software (National Institutes of Health) with β-actin serving as the loading control for normalization.

*ICC*. MIA PaCa-2 and AsPC-1 cells were seeded onto coverslips in 24-well plates at a density of $5x10^4$ cells per well and cultured for 24 h. Cells were then treated with 0.25 $\mu$mol/l GEM, 4 $\mu$mol/l SSD, their combination G0.25 + S4 or vehicle control (0.1% DMSO) for 48 h at 37˚C. After treatment, cells were fixed with 4% PFA at 4˚C for 20 min, permeabilized with 0.3% Triton X-100 for 15 min at room temperature, washed with PBS, and incubated with 3% $H_2O_2$ in deionized water at 37˚C for 10 min to quench endogenous peroxidase activity. Blocking was performed with 5% BSA (product no. A8020; Sigma-Aldrich; Merck KGaA) for 20 min at room temperature. The following primary antibodies from Proteintech Group, Inc., were applied overnight at 4˚C: Mouse monoclonal anti-Bax (1:500; 60267-1-Ig), rabbit polyclonal anti-Bcl-2 (1:1,000; 12789-1-AP), mouse monoclonal anti-cleaved caspase-3 (1:1,000; cat. no. 66470-2-Ig), mouse monoclonal anti-p-AKT (Ser473) (1:500; 66444-1-Ig) and mouse monoclonal anti-p-mTOR (Ser2448) (1:2,000; 67778-1-Ig). The next day, samples were incubated with HRP-conjugated goat anti-mouse (1:5,000; SA00001-1; Proteintech Group, Inc.) or goat anti-rabbit (1:5,000; SA00001-2; Proteintech Group, Inc.) secondary antibodies for 1.5 h at room temperature. After three washes with TBST, signals were developed using 3,3'-diaminobenzidine (DAB). DAB development was monitored in real-time under a Nikon Eclipse Ti2 light microscope (Nikon Corporation), and the reaction was stopped by rinsing with pure water once moderate brown cytoplasmic staining became visible. Nuclei were counterstained with hematoxylin for 3 min at room temperature, followed by washing and dehydration. Coverslips were mounted with neutral resin and observed under a light microscope. Images were captured and analyzed using NIS-Elements software (v5.30; Nikon Corporation). Each experiment included a negative control with non-immune IgG and a vehicle-treated DMSO control.

*Statistical analysis*. GraphPad Prism 9.0 software (Dotmatics) was used for all statistical analyses and graphing. Based on an a priori power analysis using G*Power 3.1 (ANOVA: Effect size f=0.4, $\alpha$=0.05, power=0.8), five independent biological replicates (n=5) per group were performed to ensure adequate statistical power. Prior to analysis, data normality and variance homogeneity were assessed using the Shapiro-Wilk test and Brown-Forsythe test, respectively. To account for multiple comparisons, all P-values were adjusted using the Benjamini-Hochberg correction (false discovery rate <0.05). Effect sizes with 95% CIs were calculated through bootstrap resampling (1,000 iterations). Data are presented as the mean ± standard deviation. An adjusted P-value <0.05 was considered to indicate a statistically significant difference. Specific statistical tests were applied based on the experimental design: Two-way ANOVA with Tukey's post hoc test was used to compare cell viability across time points and treatments; one-way ANOVA with Tukey's post hoc test was used for multiple group comparisons at a single time point. Effect sizes are reported as partial $\eta^2$ for ANOVA. Non-parametric alternatives (Kruskal-Wallis test with Dunn's post hoc test) were used when parametric assumptions were violated.

## Results

*SSD inhibits pancreatic cancer cell proliferation in a concentration-dependent manner*. To determine the sensitivity of MIA PaCa-2 and AsPC-1 cells to SSD (Fig. 1A), cell proliferation was examined using a CCK-8 assay. Treatment with a concentration range of 0-12 $\mu$mol/l SSD (where 0 $\mu$mol/l represents the vehicle control group) for 24-72 h significantly inhibited the proliferation of both cell lines in a concentration-dependent

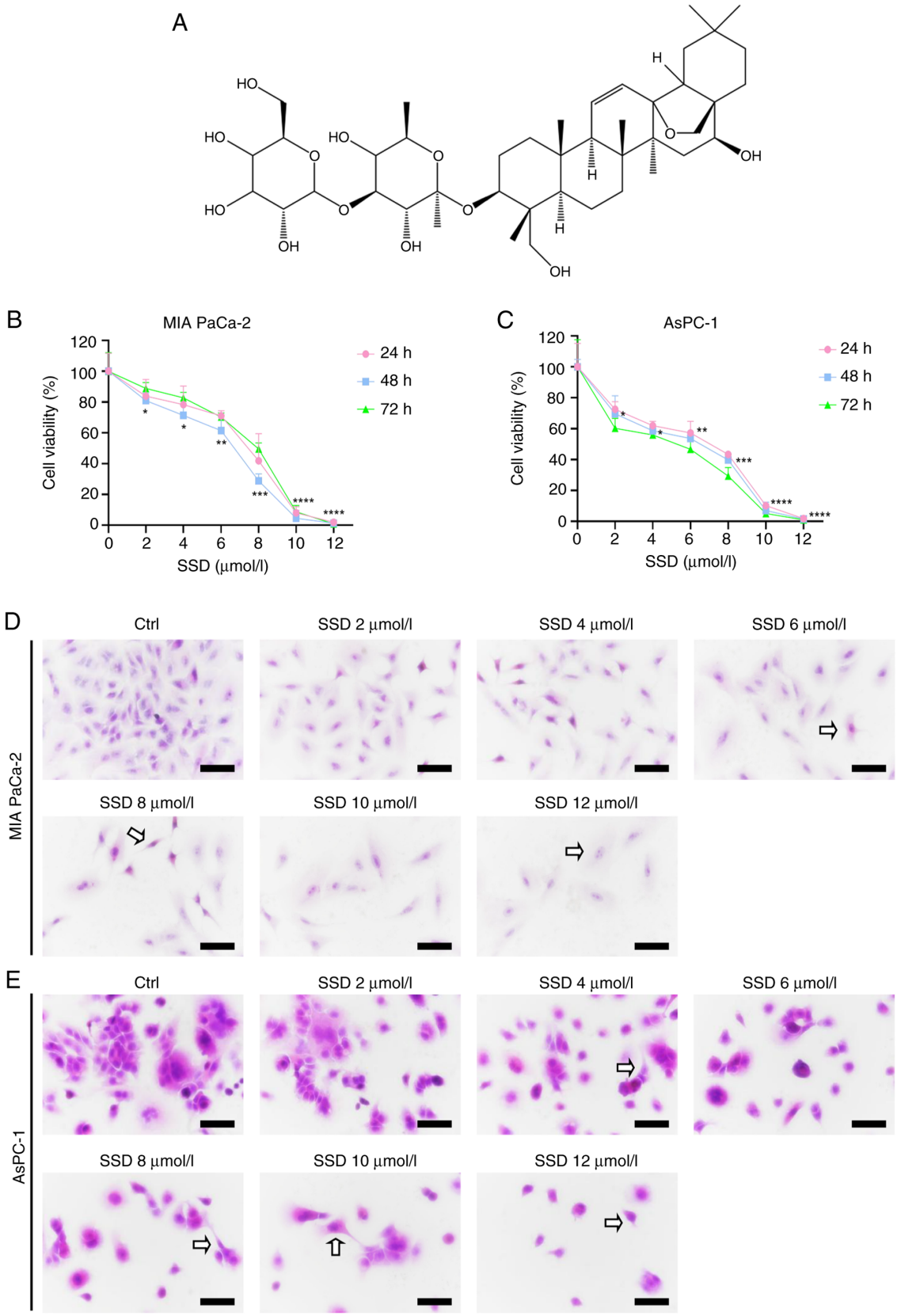


Figure 1. Dose-dependent effects of SSD on pancreatic cancer cells. (A) Chemical structure of SSD. (B) MIA PaCa-2 and (C) AsPC-1 cell viability after treatment with various concentrations of SSD (0-12 $\mu$mol/l; 24-72 h; Cell Counting Kit-8 assay). The Ctrl group was treated with 0 $\mu$mol/l SSD. Morphological changes in (D) MIA PaCa-2 and (E) AsPC-1 cells based on H&E staining (magnification, x40). Arrows point to SSD-induced apoptotic alterations, including nuclear condensation, cytoplasmic shrinkage and apoptotic bodies. Data are presented as the mean ± SD (n=5). At the 48-h mark, S12 sharply reduced cell viability in MIA PaCa-2 cells. The same effect was observed in AsPC-1 cells, where S12 also significantly inhibited cell proliferation. The statistical details for S12 are as follows: MIA PaCa-2 cells, $P_{adj}<0.0001$; $\eta^2=0.73$; and AsPC-1 cells, $P_{adj}<0.0001$; $\eta^2=0.81$. All P-values were adjusted using the Benjamini–Hochberg method. Scale bar, 50 $\mu$m. The significance indicators in (B and C) ($^{*}P<0.05$, $^{**}P<0.01$, $^{***}P<0.001$, $^{****}P<0.0001$) represent the comparison between each SSD-treated group and the Ctrl group (0 $\mu$mol/l). Statistical analysis was performed using one-way ANOVA followed by Tukey's post hoc test. Ctrl, control; SSD, Saikosaponin D.

manner (Fig. 1B and C). Specifically, significant decreases were observed starting at 2 $\mu$mol/l after 48 h, with viability falling to <20% of the control at 10 $\mu$mol/l. The sensitivity to SSD treatment was greater in AsPC-1 cells than in MIA PaCa-2 cells, as evidenced by their lower survival rates of 58.65% at 4 $\mu$mol/l and 53.60% at 6 $\mu$mol/l after 48 h of treatment, compared with 71.37 and 61.48% for MIA PaCa-2 cells at the respective concentrations (Fig. 1B and C). Concurrently, H&E staining demonstrated concentration-dependent morphological alterations, showing mild cytoplasmic shrinkage and reduced cell density at 2-4 $\mu$mol/l, and pronounced nuclear condensation, apoptotic body formation and widespread cell detachment at higher concentrations (6-12 $\mu$mol/l) in both cell lines (Fig. 1D and E).

*GEM exhibits time- and concentration-dependent growth inhibitory effects on pancreatic cancer cells*. To evaluate the sensitivity of MIA PaCa-2 and AsPC-1 cells to GEM (Fig. 2A), cells were treated with various concentrations of GEM (0, 0.25, 0.5, 1, 2, 4 and 8 $\mu$mol/l) for 24, 48 or 72 h. CCK-8 assay results demonstrated that GEM significantly suppressed the proliferation of both cell lines in a time- and concentration-dependent manner (Fig. 2B and C), as determined by one-way ANOVA with Tukey's post hoc test comparing each concentration group to the vehicle control (0 $\mu$mol/l) at each time point. Both cell lines exhibited reduced proliferation capacity after treatment with 0.25 $\mu$mol/l GEM; specifically, after 24, 48 and 72 h of exposure, the viability of MIA PaCa-2 cells decreased to 75.75, 74.68 and 72.44%, respectively, while that of AsPC-1 cells decreased to 74.80, 69.22 and 63.59%, respectively. Based on this significant growth inhibition observed at 0.25 $\mu$mol/l and to model a sub-lethal chemotherapeutic pressure, this concentration of GEM (denoted as G0.25) was selected for subsequent combination experiments. Similarly, SSD concentrations of 4 and 6 $\mu$mol/l (denoted as S4 and S6, respectively) were chosen for combination treatments as they induced moderate yet significant growth inhibition (Fig. 1B and C) while maintaining low cytotoxicity, making them suitable for evaluating synergistic effects with GEM. H&E staining further confirmed dose-dependent morphological alterations induced by GEM (0.25-8 $\mu$mol/l), including mild cytoplasmic shrinkage and reduced cell density at lower concentrations (0.25-1 $\mu$mol/l), and marked nuclear condensation, apoptotic body formation and cell detachment at higher doses (2-8 $\mu$mol/l) in both cell lines (Fig. 2D and E).

*SSD significantly enhances the anti-proliferative effects of GEM in pancreatic cancer cells through synergistic growth inhibition*. The inhibitory effects of 24-, 48- and 72-h treatments with low-dose SSD and GEM (G0.25 and S4) on the proliferation of MIA PaCa-2 and AsPC-1 cells were examined. CCK-8 assay results revealed that after 48 h of combined treatment (G0.25 + S4), the viability of MIA PaCa-2 and AsPC-1 cells was significantly inhibited compared with the Ctrl group (Fig. 3A and B). The combination therapy exhibited a stronger inhibitory effect than either monotherapy, as evidenced by the lower cell viability values. The synergistic enhancement of the anti-proliferative effect of GEM by SSD is further quantified in Table I. For both MIA PaCa-2 and AsPC-1 cells, the addition of SSD (S4 or S6) to a sub-lethal dose of GEM (G0.25) markedly reduced cell survival rates beyond the level achieved by GEM alone.

To further demonstrate the inhibitory effect of SSD combined with GEM on the proliferation of pancreatic cancer cell lines, H&E staining and colony formation assays were performed. H&E staining was performed to observe morphological changes in MIA PaCa-2 and AsPC-1 cells treated with SSD, GEM or their combination. The results showed that the proliferation of both pancreatic cancer cell lines was inhibited, accompanied by a reduction in cell number, cell shrinkage, rounding, chromatin condensation, increased cell debris and formation of apoptotic bodies (Fig. 3C). Colony formation assay results showed that the combined treatment group (G0.25 + S4) exhibited significantly reduced colony formation compared with the corresponding single-drug GEM group (Fig. 3D). In MIA PaCa-2 and AsPC-1 cells treated with SSD + GEM (G0.25 + S4), the colony formation rates decreased by 32.6 and 23.4%, respectively, compared with the corresponding single-drug GEM groups (Fig. 3E and F).

*Synergistic induction of apoptosis by SSD and GEM in pancreatic cancer cells through modulation of apoptotic proteins*. TUNEL assays were subsequently performed to evaluate the effect of SSD, GEM and combined SSD + GEM treatment on the apoptosis of MIA PaCa-2 and AsPC-1 cells. The results showed that when applied alone, SSD and GEM induced modest, albeit significant, increases in TUNEL fluorescence intensity in both cell lines (Fig. 4A). However, the combined SSD + GEM treatment for 48 h induced a significantly stronger apoptotic response compared with GEM monotherapy in both MIA PaCa-2 and AsPC-1 cells (Fig. 4B and C; $P_{adj}<0.001$), suggesting a synergistic interaction. This suggested that SSD may act synergistically with GEM to induce apoptosis in pancreatic cancer cells. Apoptotic features were next verified by Hoechst 33258 staining, which revealed brightly stained, irregularly shaped, dense nuclei characteristic of apoptotic cells (Fig. 4D).

In addition, ICC analysis revealed distinct protein expression patterns of key apoptotic regulators; specifically, increased expression of pro-apoptotic Bax and cleaved caspase-3, alongside decreased expression of anti-apoptotic Bcl-2-in SSD + GEM-treated pancreatic cancer cells compared with GEM-only treated controls (Fig. 5A). These ICC findings were further corroborated by western blot analysis (Fig. 5B). The combination treatment potently altered the levels of apoptosis-related proteins relative to the control. Specifically, it increased the levels of Bax and cleaved caspase-3, while decreasing the levels of Bcl-2 and total caspase-3 in both cell lines (Fig. 5C and D). These consistent results from both ICC and western blot analyses demonstrated that SSD not only induced apoptosis in pancreatic cancer cells but also enhanced the pro-apoptotic effect of GEM by modulating key apoptotic regulators. The observed changes in protein expression levels shown in Fig. 5C and D are consistent with a synergistic enhancement of apoptosis by the combination treatment.

To quantitatively validate the mechanistic synergy between GEM and SSD, drug interaction was analyzed using the Chou-Talalay method. This analysis confirmed robust synergistic effects across multiple cellular endpoints (data not shown). Specifically, the calculated CI values were consistently

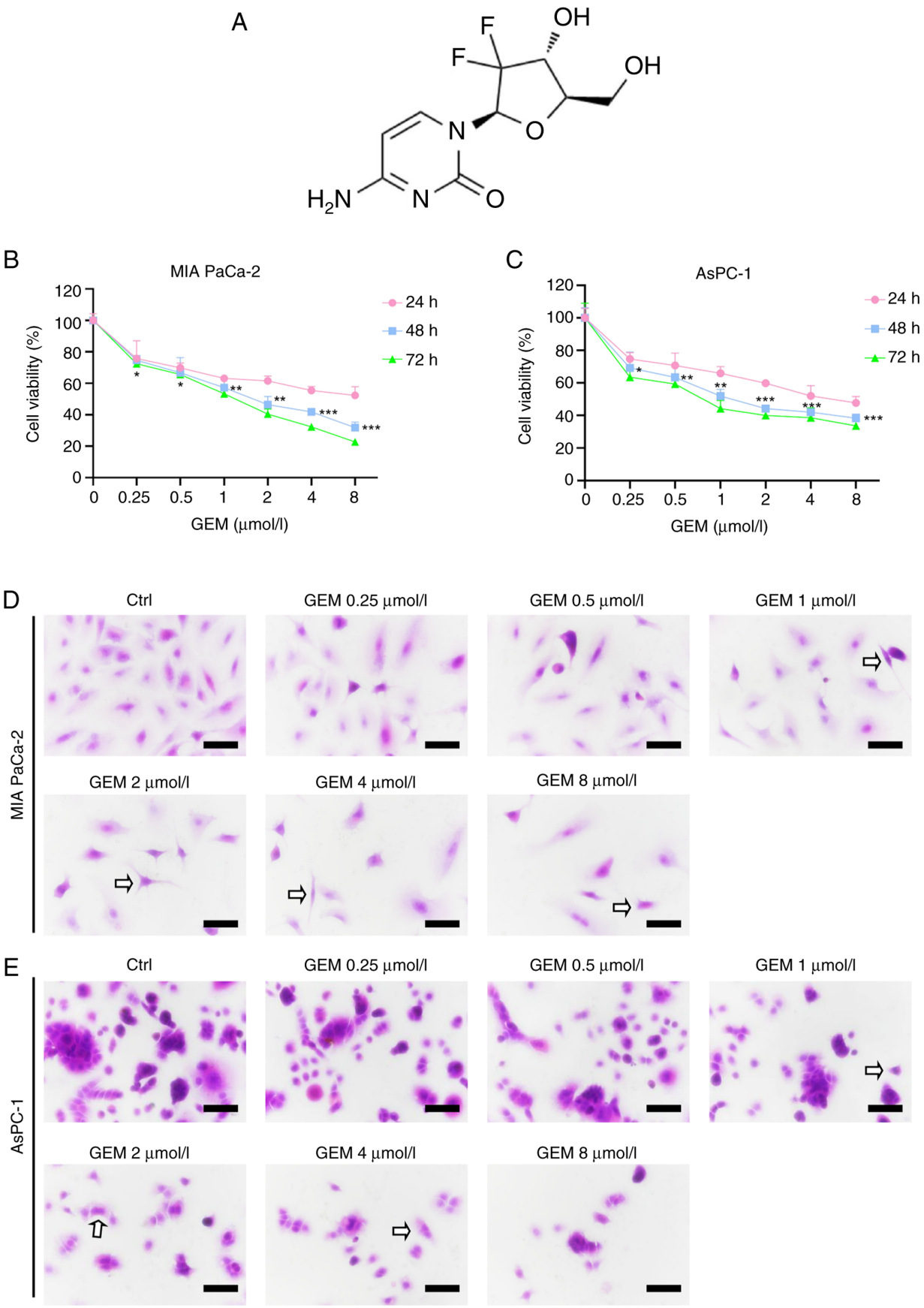


Figure 2. Dose- and time-dependent effects of GEM on pancreatic cancer cells. (A) Chemical structure of GEM. Viability of (B) MIA PaCa-2 and (C) AsPC-1 cells treated with various concentrations of GEM (0-8 $\mu$mol/l; 24-72 h; Cell Counting Kit-8 assay). The Ctrl group was treated with 0 $\mu$mol/l GEM. Representative H&E staining images of (D) MIA PaCa-2 and (E) AsPC-1 cells (magnification, x40). Arrows indicate GEM-induced morphological alterations characteristic of apoptosis. Data are presented as the mean ± SD (n=5). All P-values were adjusted using the Benjamini-Hochberg method. The significance indicators in (B and C) ($^{*}$P<0.05, $^{**}$P<0.01, $^{***}$P<0.001) represent the comparison between each GEM-treated group and the Ctrl group (0 $\mu$mol/l) at the same time point. Statistical analysis was performed using one-way ANOVA followed by Tukey's post hoc test. Scale bar, 50 $\mu$m. Ctrl, control; GEM, gemcitabine.

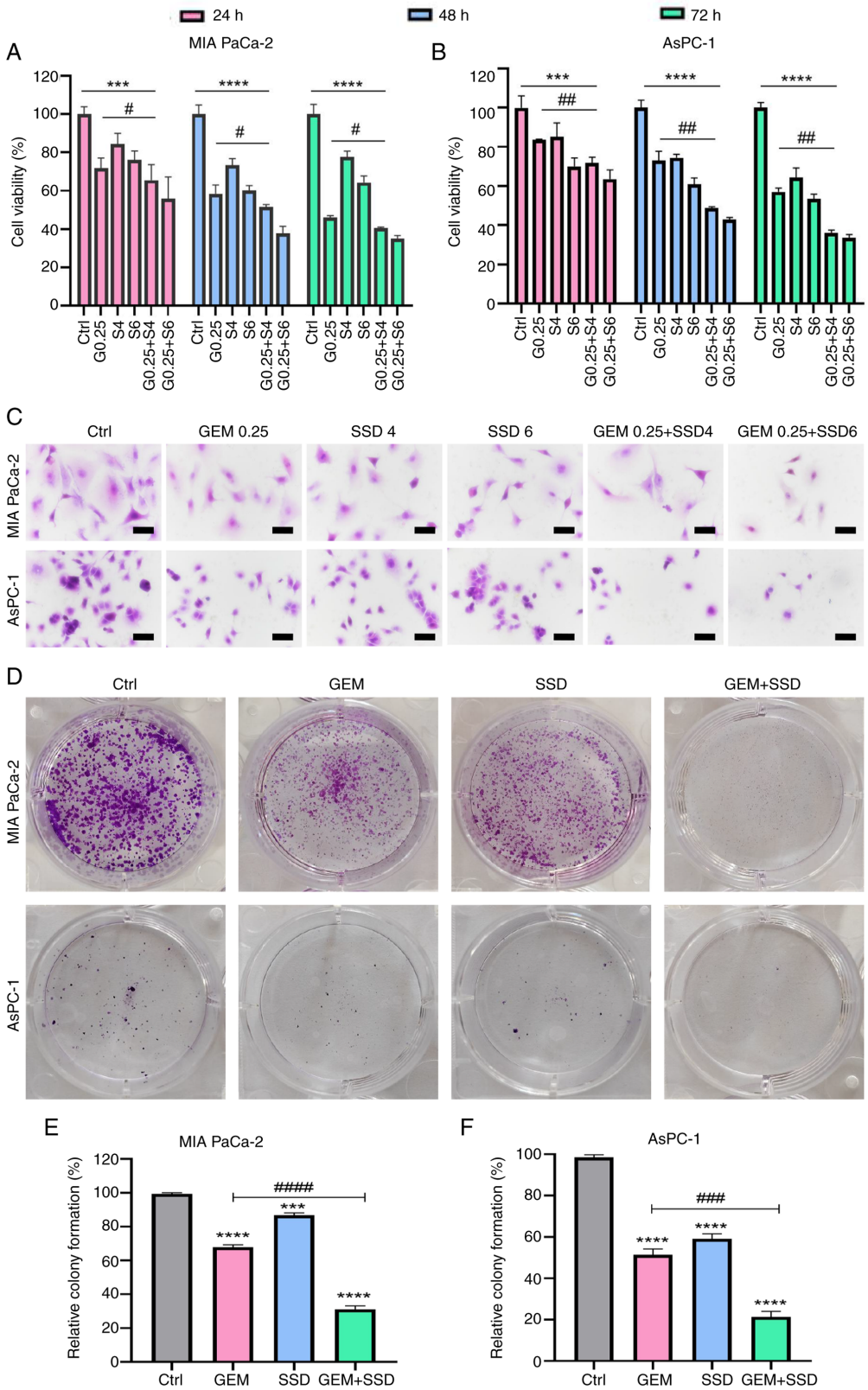


Figure 3. Combinatorial effects of GEM and SSD on pancreatic cancer cells. Viability of (A) MIA PaCa-2 and (B) AsPC-1 cells treated with G0.25, S4, S6 or combinations (G0.25 + S4/S6) for 24-72 h. (C) H&E staining showing morphological changes (magnification, x40). Scale bar, 50 $\mu$m. (D-F) Colony formation assays. (D) Representative images, and quantification in (E) MIA PaCa-2 and (F) AsPC-1 cells. (D-F) GEM, 0.25 $\mu$mol/l and SSD, 4 $\mu$mol/l. The colony formation rate for each group is expressed as a percentage relative to the untreated control (Ctrl) group, which was set to 100%. Note that the absolute colony-forming capacity of the Ctrl group under baseline culture conditions was defined as the reference point. Data are presented as the mean ± SD (n=5). The data demonstrate that the combination treatment (G0.25 + S4) resulted in significantly enhanced antitumor effects compared with GEM monotherapy (G0.25). With regard to cell viability, the combination was significantly more effective ($P_{adj}$=0.003; effect size: $\eta^2$=0.62; 95% CI, 0.41-0.79). A strong synergistic effect was also observed in the colony formation assay, where the combination treatment led to a marked reduction in clonogenic survival ($P_{adj}$=0.001; effect size, $\eta^2$=0.68; 95% CI, 0.46-0.83). All P-values are Benjamini-Hochberg-adjusted. $^{***}$P<0.001, $^{****}$P<0.0001 for comparisons vs. Ctrl; $^{\#}$P<0.05, $^{\#\#}$P<0.01, $^{\#\#\#}$P<0.001, $^{\#\#\#\#}$P<0.0001 for G0.25 + S4 vs. G0.25. Statistical analysis was performed using two-way ANOVA with Tukey's post hoc test (A and B) and one-way ANOVA with Tukey's post hoc test (E and F). Ctrl, control; GEM, gemcitabine; SSD, Saikosaponin D; G0.25, 0.25 $\mu$mol/l GEM; SX, X $\mu$mol/l SSD.

Table I. Growth inhibitory effects of combined GEM + SSD exposure on pancreatic cancer cell lines.

| | Cell survival rate, % | | |
|---|---|---|---|
| Cell line | G0.25 | G0.25 + S4 | G0.25 + S6 |
| MIA PaCa-2 | 69.22 | 56.97[a] | 40.65[a] |
| AsPC-1 | 74.68 | 45.64[b] | 42.13[b] |

[a]P<0.05, [b]P<0.01 compared with the G0.25 group (one-way ANOVA with Tukey's post hoc test). Data are presented as the mean cell survival rate from five independent experiments (n=5). GEM, gemcitabine; G0.25, 0.25 $\mu$mol/l GEM; SSD, Saikosaponin D; S4, 4 $\mu$mol/l SSD; S6, 6 $\mu$mol/l SSD.

below the synergy threshold (CI<1) in both pancreatic cancer cell lines, indicating pharmacological synergy. These results further support the conclusion that SSD enhances the efficacy of GEM through synergistic inhibition of cell viability and induction of apoptosis.

*SSD potentiates the antitumor effects of GEM through enhanced AKT/mTOR suppression*. The involvement of AKT/mTOR signaling in pancreatic cancer progression is well established (14,21). To investigate whether SSD mediates its effects through this pathway, ICC analysis was first performed. As shown in Fig. 6A, ICC staining demonstrated markedly reduced cytoplasmic levels of p-AKT and p-mTOR in SSD + GEM-treated cells compared with either single-agent treatment or control groups, with more pronounced inhibition observed in AsPC-1 cells than in MIA PaCa-2 cells. These ICC findings were semi-quantitatively confirmed by western blot analysis (Fig. 6B). SSD treatment alone exhibited comparable inhibition of p-AKT and p-mTOR levels to GEM monotherapy. However, the combination treatment exerted significantly greater suppressive effects compared with GEM alone, as quantified by western blot analysis (Fig. 6C and D). Densitometric evaluation revealed a reduction in the p-AKT/AKT ratio by 42.3% in MIA PaCa-2 cells and 72.1% in AsPC-1 cells. Similarly, the p-mTOR/mTOR ratio was reduced by 51.4 and 80.3% in MIA PaCa-2 and AsPC-1 cells, respectively. Notably, AsPC-1 cells exhibited more substantial pathway inhibition than MIA PaCa-2 cells across both detection methods. These consistent results from complementary techniques demonstrated that SSD effectively suppressed AKT/mTOR signaling in pancreatic cancer cells, with enhanced inhibition when combined with GEM. The combination treatment (G0.25 + S4) resulted in significantly greater inhibition of both the p-AKT/AKT and p-mTOR/mTOR ratios compared with GEM alone (G0.25), with these effects being consistently more pronounced in AsPC-1 cells (Fig. 6C and D). The inhibition was statistically significant for both the p-AKT/AKT ratio ($P_{adj}$<0.0001; $\eta^2$=0.73; 95% CI, 0.55-0.86) and the p-mTOR/mTOR ratio ($P_{adj}$<0.0001; $\eta^2$=0.81; 95% CI, 0.67-0.91).

*SSD promotes autophagy in pancreatic cancer cells*. The interconnected roles of autophagy and apoptosis in cancer regulation are well documented (28-32). Having observed SSD-induced apoptosis in pancreatic cancer cells, the present study next investigated its potential to induce autophagy. Initial assessment by MDC staining revealed substantial accumulation of autophagic vesicles in both MIA PaCa-2 and AsPC-1 cells following treatment. While single-agent SSD or GEM treatment increased autophagic activity, the combination therapy exerted markedly greater effects, substantially elevating MDC fluorescence intensity in both MIA PaCa-2 and AsPC-1 cells compared with GEM alone (Fig. 7A). ICC analysis corroborated these findings, demonstrating increased cytoplasmic expression of autophagy markers Beclin 1 and LC3 in cells treated with the SSD and GEM combination (G0.25 + S4) (Fig. 7B). The intensity and distribution of staining were most pronounced in the SSD + GEM combination groups, consistent with the MDC results. Western blotting semi-quantification provided precise molecular characterization of these effects (Fig. 7C). Treatment with the SSD and GEM combination (G0.25 + S4) elevated both Beclin 1 expression and the LC3II/LC3I ratio compared with GEM alone, with Beclin 1 expression increasing by 33.5% in MIA PaCa-2 cells and 42.3% in AsPC-1 cells, and the LC3II/LC3I ratio increasing by 48.1% in MIA PaCa-2 cells and 56.7% in AsPC-1 cells (Fig. 7D and E). The combination treatment showed additive effects across all autophagy markers, with AsPC-1 cells again exhibiting greater sensitivity than MIA PaCa-2 cells. These complementary analyses demonstrated that SSD not only induced autophagy in pancreatic cancer cells but synergistically enhanced GEM-mediated autophagy activation through inhibition of the AKT/mTOR pathway (Fig. 8), potentially contributing to the observed antitumor efficacy of the combination therapy. The combination treatment (G0.25 + S4) significantly enhanced autophagic activity compared with GEM (G0.25) alone. Specifically, it increased the LC3II/LC3I ratio ($P_{adj}$=0.001; $\eta^2$=0.65; 95% CI, 0.43-0.81) and elevated Beclin 1 expression ($P_{adj}$=0.002; $\eta^2$=0.59; 95% CI, 0.36-0.77).

## Discussion

Pancreatic cancer is one of the most lethal malignant tumors, and is often described as the most aggressive of all cancers due to its highly metastatic nature, coupled with high mortality, low early detection and poor survival rates (1,33). In recent years, the incidence and mortality of pancreatic cancer have continued to rise worldwide (34). Although GEM monotherapy or combination therapy with other agents is widely used as a first-line treatment for pancreatic cancer, the prognosis remains poor due to the rapid development of drug resistance *in vivo* (35). Therefore, there is an urgent need to

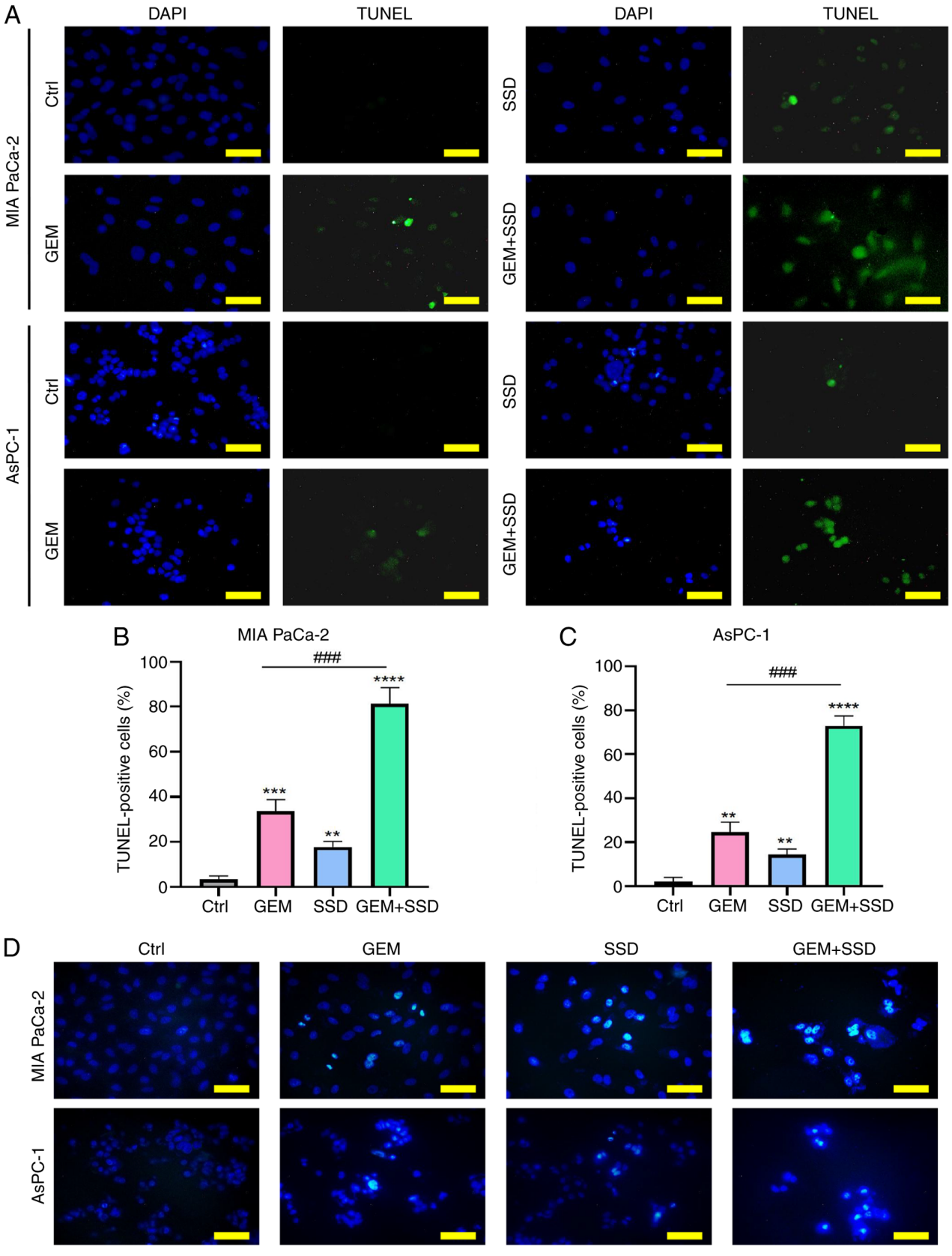


Figure 4. Apoptosis induction by GEM and SSD combination therapy. (A) Representative TUNEL/DAPI staining images (green, apoptotic cells; blue, nuclei) in MIA PaCa-2 (top) and AsPC-1 (bottom) cells treated with Ctrl, G0.25, S4 or the combination (G0.25 + S4). Quantification of TUNEL-positive cells in (B) MIA PaCa-2 and (C) AsPC-1 cells. (D) Hoechst 33258 staining showing apoptotic nuclei with condensed chromatin. In the figure, GEM represents 0.25 $\mu$mol/l GEM and SSD represents 4 $\mu$mol/l SSD. Data are presented as the mean ± SD (n=5). The data show that the combination treatment (G0.25 + S4) significantly enhanced the induction of apoptosis compared with GEM monotherapy (G0.25). The combination treatment significantly increased apoptosis, evidenced by a substantial rise in TUNEL-positive cells ($P_{adj}$=0.002; $\eta^2$=0.59; 95% CI, 0.36-0.77) and a corresponding increase in condensed chromatin, a hallmark of apoptosis, as shown by Hoechst 33258 staining ($P_{adj}$=0.004; $\eta^2$=0.55; 95% CI, 0.31-0.74). All P-values are Benjamini-Hochberg-adjusted. Scale bar, 50 $\mu$m. $^{**}$P<0.01, $^{***}$P<0.001, $^{****}$P<0.0001 for comparisons vs. Ctrl; $^{###}$P<0.001 for G0.25 + S4 vs. G0.25. Statistical analysis was performed using one-way ANOVA with Tukey's post hoc test for multiple comparisons. Ctrl, control; GEM, gemcitabine; SSD, Saikosaponin D.

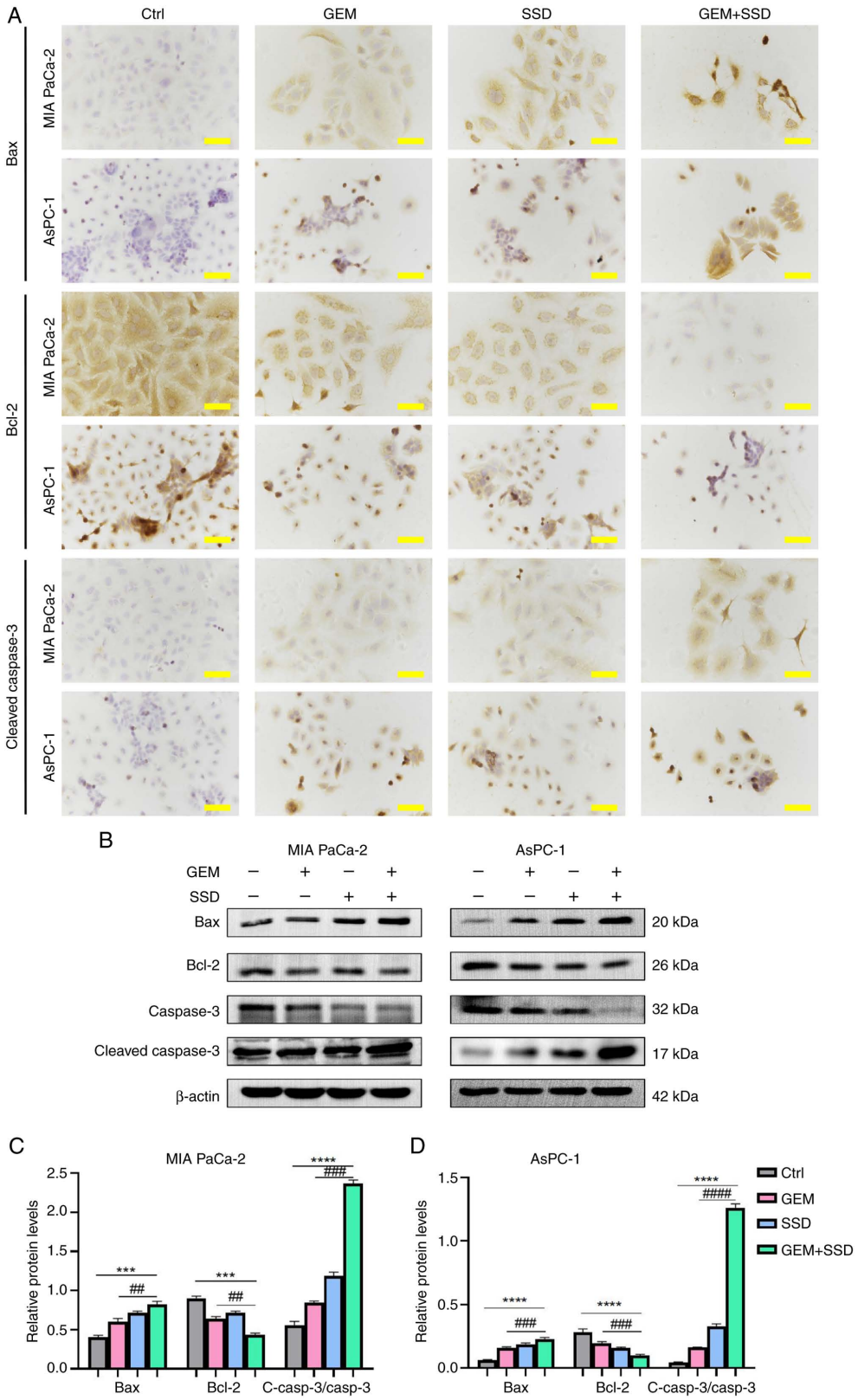


Figure 5. Molecular mechanisms of apoptosis induction by GEM and SSD combination treatment. (A) Immunocytochemistry of MIA PaCa-2 and AsPC-1 cells treated with Ctrl, G0.25, S4 or the combination (G0.25 + S4; magnification, x40). Scale bar, 50 $\mu$m. (B) Western blot analysis of apoptosis markers Bax (20 kDa), Bcl-2 (26 kDa), caspase-3 (32 kDa) and cleaved caspase-3 (17 kDa), and β-actin (42 kDa). Semi-quantification of immunoblots for (C) MIA PaCa-2 and (D) AsPC-1 cells. In the figure, GEM represents 0.25 $\mu$mol/l GEM and SSD represents 4 $\mu$mol/l SSD. Data are presented as the mean ± SD (n=5). The combination treatment (G0.25 + S4) increased the expression of pro-apoptotic Bax and cleaved caspase-3, and elevated the c-Casp3/Casp3 ratio, while decreasing the expression of anti-apoptotic Bcl-2 compared with GEM monotherapy (G0.25). Specifically, Bax expression increased by 2.3-fold in MIA PaCa-2 cells and 3.1-fold in AsPC-1 cells. Conversely, Bcl-2 expression was reduced to 45 and 38% of GEM monotherapy levels in MIA PaCa-2 and AsPC-1 cells, respectively. The c-Casp3/Casp3 ratio was significantly enhanced by the combination treatment, indicating robust activation of the apoptotic executioner pathway. All P-values are Benjamini-Hochberg-adjusted. $^{***}$P<0.001, $^{****}$P<0.0001 for G0.25 + S4 vs. Ctrl; $^{\#\#}$P<0.01, $^{\#\#\#}$P<0.001, $^{\#\#\#\#}$P<0.0001 for G0.25 + S4 vs. G0.25. Statistical analysis was performed using one-way ANOVA with Tukey's post hoc test for multiple comparisons. Ctrl, control; GEM, gemcitabine; SSD, Saikosaponin D; Casp3, caspase-3; c-Casp3, cleaved caspase-3.

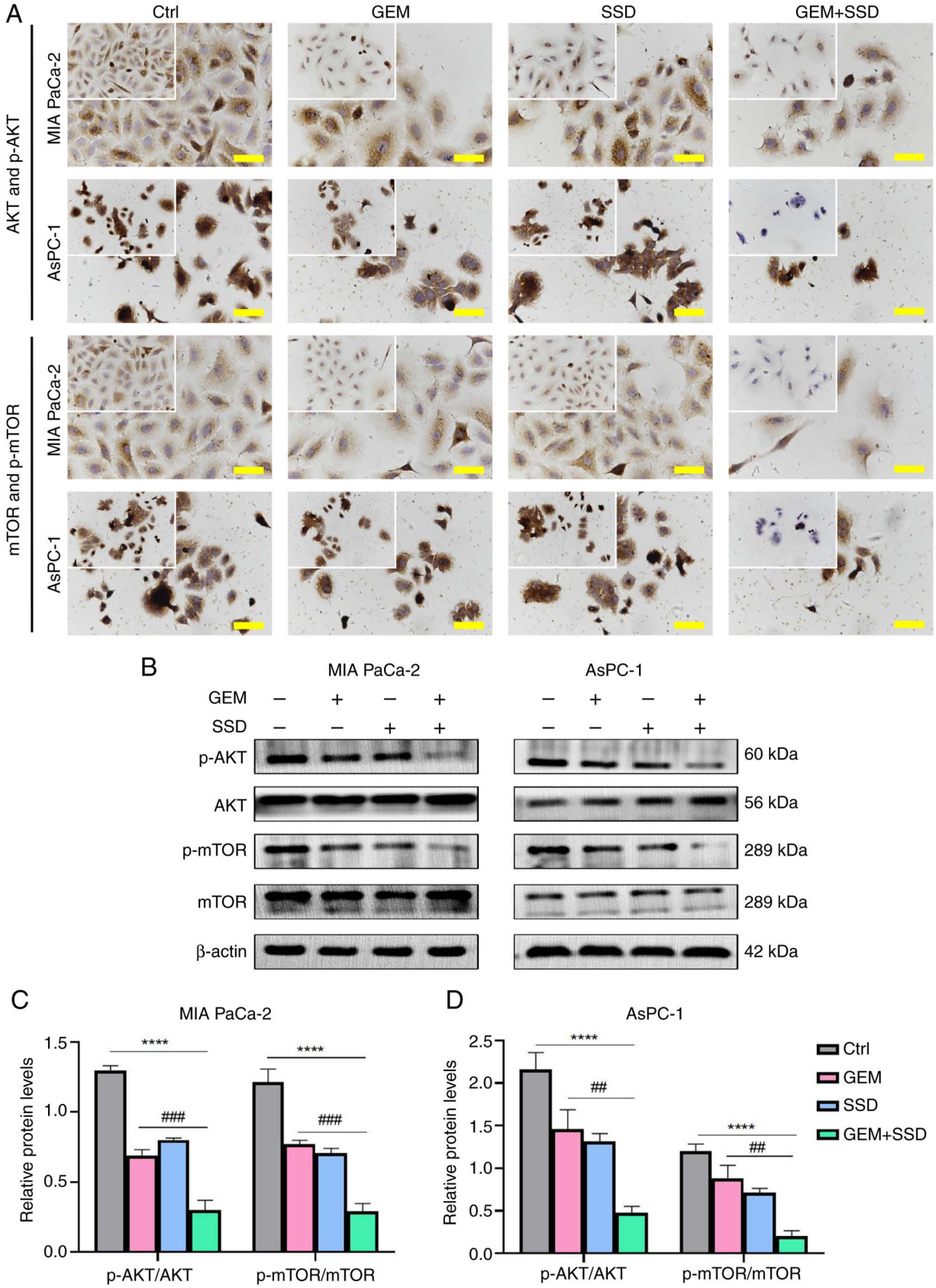


Figure 6. AKT/mTOR pathway inhibition by GEM and SSD combination therapy. (A) Immunocytochemistry staining of AKT/mTOR signaling proteins in MIA PaCa-2 and AsPC-1 cells treated with Ctrl, G0.25, S4 or the combination (G0.25 + S4; magnification, x40; insets show phosphoprotein details). Scale bar, 50 $\mu$m. (B) Western blot analysis of p-AKT (60 kDa), AKT (56 kDa), p-mTOR (289 kDa), mTOR (289 kDa) and β-actin (42 kDa). Semi-quantification of phosphorylation ratios in (C) MIA PaCa-2 and (D) AsPC-1 cells. In the figure, GEM represents 0.25 $\mu$mol/l GEM and SSD represents 4 $\mu$mol/l SSD. Data are presented as the mean ± SD (n=5). Compared with GEM monotherapy, the G0.25 + S4 combination led to a greater reduction in both p-AKT/AKT and p-mTOR/mTOR ratios (both $P_{adj}$<0.0001), with large effect sizes ($\eta^2$=0.73 and 0.81, respectively). All P-values are Benjamini-Hochberg-adjusted. $^{****}$P<0.0001 for G0.25 + S4 vs. Ctrl; $^{##}$P<0.01, $^{###}$P<0.001 for G0.25 + S4 vs. G0.25. Statistical analysis was performed using one-way ANOVA with Tukey's post hoc test. Ctrl, control; GEM, gemcitabine; SSD, Saikosaponin D; p-, phosphorylated.

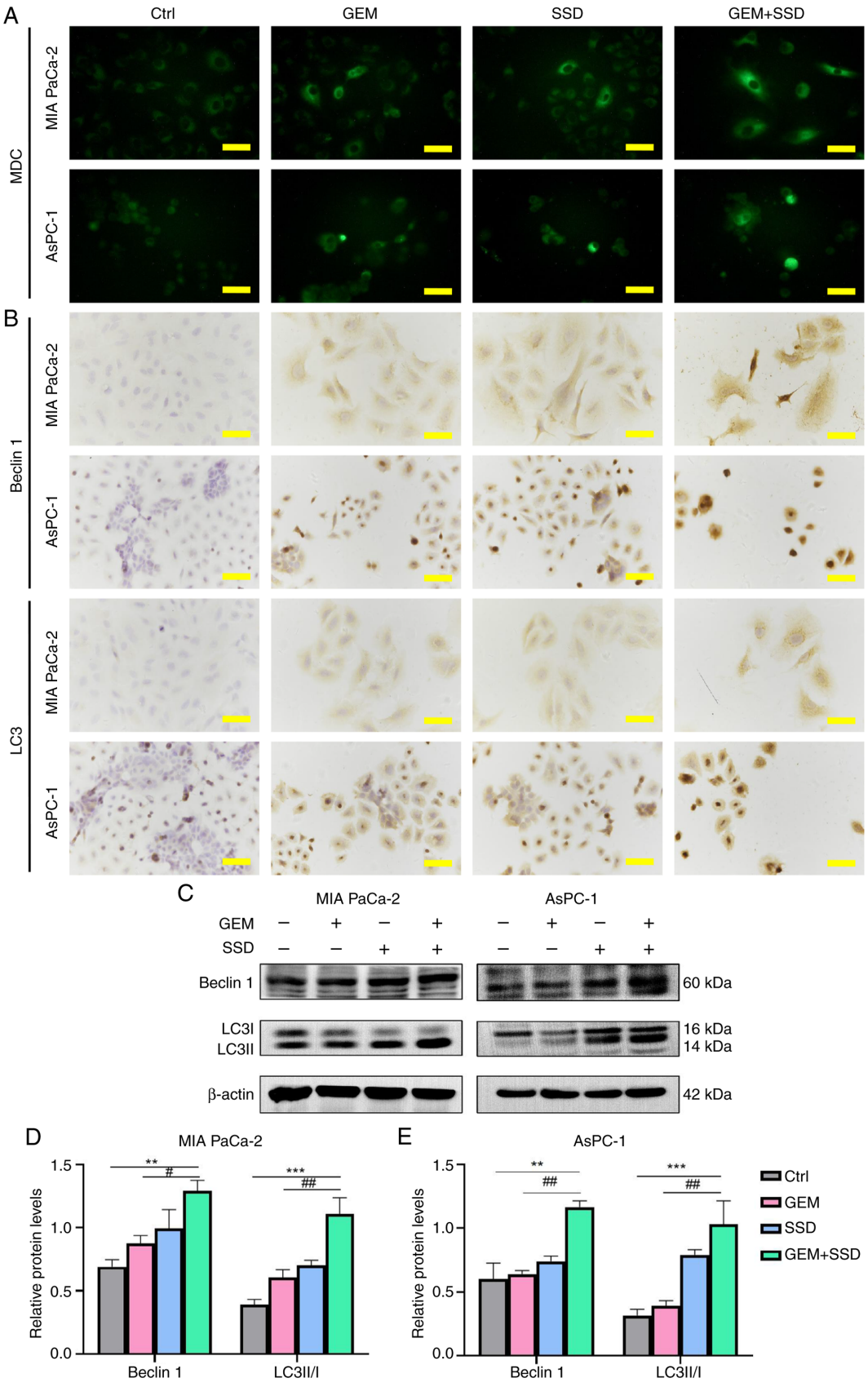


Figure 7. Autophagy induction by GEM and SSD combination treatment. (A) MDC staining (green) showing autophagosome accumulation in MIA PaCa-2 and AsPC-1 cells treated with Ctrl, G0.25, S4 or the combination (G0.25 + S4; magnification, x40). (B) Immunocytochemistry of autophagy markers. (C) Western blot analysis of Beclin 1 (60 kDa), LC3I (16 kDa), LC3II (14 kDa) and β-actin (42 kDa). Semi-quantification of autophagy markers in (D) MIA PaCa-2 and (E) AsPC-1 cells. In the figure, GEM represents 0.25 $\mu$mol/l GEM and SSD represents 4 $\mu$mol/l SSD. Data are presented as the mean ± SD (n=5). Compared with GEM monotherapy, the G0.25 + S4 combination significantly increased the LC3-II/I ratio ($P_{adj}$=0.001; $\eta^2$=0.65; 95% CI, 0.43-0.81) and Beclin 1 levels ($P_{adj}$=0.002; $\eta^2$=0.61; 95% CI, 0.38-0.78), indicating strong induction of autophagy. All P-values are Benjamini-Hochberg-adjusted. Scale bar, 50 $\mu$m. $^{**}$P<0.01, $^{***}$P<0.001 for G0.25 + S4 vs. Ctrl; $^{\#}$P<0.05, $^{\#\#}$P<0.01 for G0.25 + S4 vs. G0.25. Statistical analysis was performed using one-way ANOVA with Tukey's post hoc test. Ctrl, control; GEM, gemcitabine; SSD, Saikosaponin D; MDC, monodasylcadaverine.

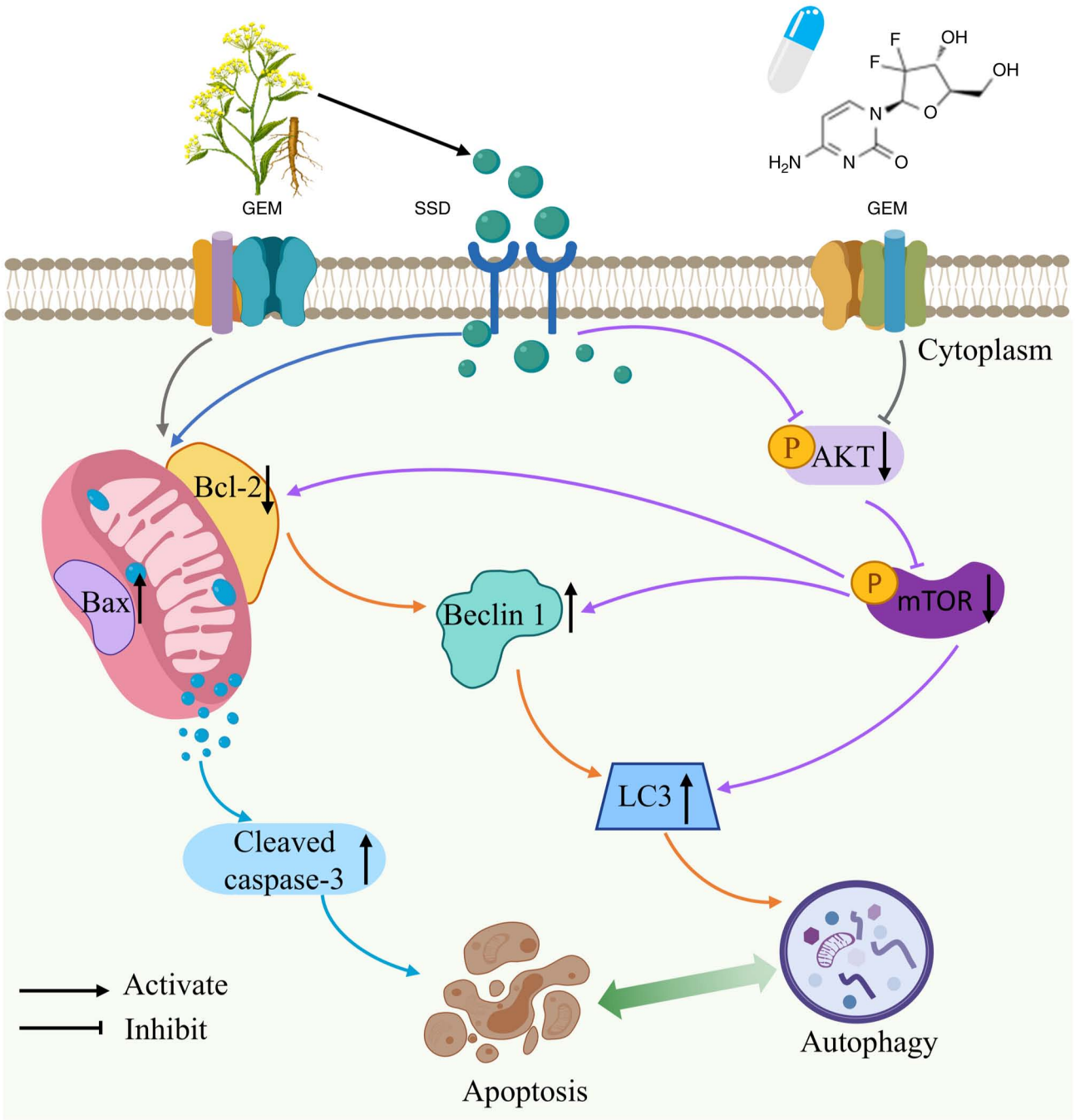


Figure 8. Proposed mechanism of GEM and SSD combination therapy. Co-treatment with GEM and SSD synergistically inhibits the AKT/mTOR pathway, concurrently inducing apoptosis (via Bax/Bcl-2 modulation and caspase-3 activation) and autophagy (via Beclin 1 activation and LC3 conversion), thereby overcoming GEM resistance in pancreatic cancer cells. GEM, gemcitabine; P, phosphorylated; SSD, Saikosaponin D.

identify or develop anticancer agents with low toxicity and high efficiency to enhance the sensitivity to GEM and improve treatment outcomes for pancreatic cancer. TCM has gained increasing attention in cancer therapy research due to its multi-target pharmacological properties and favorable safety profiles (19,36,37). Additionally, TCM formulations contain a variety of bioactive components, some of which, such as berberine, curcumin and artemisinin derivatives, have shown potential against pancreatic cancer in pre-clinical and clinical research (38,39).

SSD is a triterpenoid saponin monomer extracted from *Bupleurum chinense* roots (Radix Bupleuri), a classic TCM formula (40). SSD has antitumor, anti-inflammatory and antiviral properties, and is considered to be one of the most bioactive natural saponins (41). Furthermore, SSD has been reported to be relatively safe in an appropriate dose range (42). In the experimental treatment of glioma and certain pancreatic cancers, the typical concentration of SSD is maintained between 5-20 $\mu$mol/l, with the lowest effective dose observed at ~5 $\mu$mol/l in *in vitro* studies (25). The concentration of SSD (4 $\mu$mol/l) selected in the present study therefore falls within this safe range. The routine clinical dose of GEM is usually 1,000 mg/m$^2$ administered once a week, with a week off after several weeks of continuous use (43). In the present

study, 0.25 $\mu$mol/l was selected as a sub-lethal and biologically relevant concentration of GEM for combination treatments, based on dose-response curves demonstrating significant growth inhibition at this dose; the lowest concentration tested that produced a statistically significant anti-proliferative effect in both MIA PaCa-2 and AsPC-1 cell lines.

The present study demonstrated that low-dose SSD exposure inhibited the proliferation of pancreatic cancer cells *in vitro*, and also enhanced the antiproliferative effects of GEM in these cells. While SSD inhibited the proliferation of MIA PaCa-2 and AsPC-1 cells in a dose-dependent manner, AsPC-1 cells were more sensitive to SSD than MIA PaCa-2 cells. These effects were further demonstrated through colony formation assays, which additionally indicated increased inhibition of tumor cell clonogenic capacity following combined treatment with SSD and GEM. TUNEL and Hoechst 33258 staining assays also demonstrated that SSD induced apoptosis in both cell lines. Notably, TUNEL fluorescence estimates suggested potential synergistic effects for SSD when applied in combination with GEM. Furthermore, the combination of SSD and GEM exhibited synergistic effects on the induction of autophagy in both MIA PaCa-2 and AsPC-1 cells. These findings suggest robust potential for SSD as an adjuvant therapy for pancreatic cancer in patients treated with GEM.

The AKT/mTOR signaling pathway serves an important role in critical cellular processes, and its dysregulation contributes to tumor development and progression in numerous cancer types, as demonstrated in NSCLC (13), breast cancer (11), hepatocellular carcinoma (44) and pancreatic cancer (15). PI3K generates phosphatidylinositol (3,4,5)-trisphosphate, which binds to and recruits phosphatidylinositol-dependent protein kinase 1 and AKT to the cell membrane, thereby activating AKT. Activated AKT regulates multiple downstream targets, including mTOR and Bad, and through phosphorylation reactions, regulates a variety of cellular physiological processes such as proliferation, survival, apoptosis and metabolism (9). The association of AKT/mTOR activity with apoptosis and autophagy in cancer cells has been documented. Wang *et al* (13) demonstrated that PTPRH promoted NSCLC progression through glycolysis mediated by the PI3K/AKT/mTOR signaling pathway. Lai *et al* (42) showed that SSD inhibited proliferation and promoted apoptosis in pancreatic cancer cells via activation of the MKK4-JNK signaling pathway. In line with this evidence, the present study suggested that inhibition of the AKT/mTOR pathway underlies SSD + GEM-induced apoptosis and autophagy in pancreatic cancer cells, as demonstrated by western blotting and ICC results showing that SSD and GEM inhibited the phosphorylation of AKT and mTOR. Upon activation, AKT phosphorylates the pro-apoptotic Bad protein, preventing its binding to the anti-apoptotic proteins Bcl-2 and Bcl-XL. This results in inhibition of the pro-apoptotic protein Bax, impeding the occurrence of apoptosis. Accordingly, when AKT is inhibited, Bax activation leads to the release of cytochrome *c* from mitochondria, which activates caspase-3 (45). Caspase-3 in turn cleaves its substrate poly (ADP-ribose) polymerase, an enzyme involved in DNA repair, which accelerates the apoptotic process (46). In the present study, evidence of SSD-mediated induction of apoptosis was provided by western blotting and ICC analyses showing downregulated expression of Bcl-2 and total caspase-3, along with upregulated expression of Bax and cleaved caspase-3, following treatment with SSD, GEM or their combination. These findings suggested that SSD, both alone and in combination with GEM, inhibited pancreatic cancer cell proliferation and induced apoptosis by inhibiting the AKT/mTOR pathway.

Studies have further highlighted the pivotal role of AKT/mTOR dysregulation in pancreatic cancer chemoresistance. For instance, Mortazavi *et al* (47) highlighted that hyperactivation of PI3K/AKT/mTOR signaling not only promoted tumor survival but also mediated adaptive resistance to GEM by upregulating efflux pumps and DNA repair mechanisms. Similarly, Sheng *et al* (48) demonstrated that mTOR inhibition sensitized pancreatic cancer cells to GEM through suppression of musashi RNA binding protein 2-mediated epithelial-mesenchymal transition. Notably, Shimia *et al* (17) reported that dual targeting of AKT and mTOR synergized with conventional chemotherapy by disrupting feedback loops that sustain tumor survival. These findings align with the present results, reinforcing that AKT/mTOR inhibition of SSD could disrupt multiple resistance mechanisms, including metabolic reprogramming and anti-apoptotic signaling.

In the present study, combinatorial testing of 4 and 6 $\mu$mol/l SSD with sub-lethal GEM (0.25 $\mu$mol/l) was conducted. The 4 $\mu$mol/l SSD dose (G0.25 + S4) was chosen for detailed mechanistic analysis to investigate the basis of the synergistic effects under conditions of minimal cytotoxicity. Specifically, the 4 $\mu$mol/l SSD + GEM combination achieved proliferation inhibition comparable to that of higher doses, reducing colony formation by 29.3% in MIA PaCa-2 cells vs. 15.1% in AsPC-1 cells. Furthermore, this combination induced marked apoptosis and autophagy in MIA PaCa-2 cells, evidenced by a 61.6% increase in cleaved caspase-3 levels and a 56.7% rise in LC3-II/I ratios. The favorable safety profile of this concentration, consistent with prior applications of SSD in pancreatic models (42), further supports its suitability for prolonged mechanistic investigation. Although higher SSD doses (6 $\mu$mol/l) further reduced viability (for instance, resulting in a 31.6% decrease in survival in AsPC-1 cells treated with G0.25 + S6 at 72 h), the 4 $\mu$mol/l dose provided the best efficacy-toxicity balance, reflecting clinical strategies that prioritize minimizing chemotherapy doses through the use of sensitizing adjuvants.

While the present study demonstrated that SSD synergized with GEM primarily through AKT/mTOR inhibition, the reported effects of SSD on STAT3/Bcl-2 and IKKβ/NF-κB pathways in other cancer types (22,23), including NSCLC and gastric cancer, suggest potential parallel mechanisms in pancreatic cancer. Although these pathways were not explicitly examined in the present study, the observed upregulation of Bax and downregulation of Bcl-2 align with STAT3/Bcl-2 axis modulation, as STAT3 often transcriptionally regulates Bcl-2. Similarly, NF-κB suppression could further amplify apoptosis via caspase-3 activation (49). Future studies should dissect these interactions to fully unravel the pleiotropic antitumor effects of SSD.

Untreated MIA PaCa-2 cells exhibited detectable cleaved caspase-3 levels, consistent with their known genetic profile. This cell line carries oncogenic $KRAS^{G12J}$ and mutant $TP53^{R248W}$ (50), driving constitutive endoplasmic reticulum stress

and DNA damage responses that prime apoptotic pathways even in untreated conditions. Similar basal caspase activation has been reported in other KRAS-mutant pancreatic models (51). The present data demonstrated that SSD + GEM combination therapy further amplified cleaved caspase-3 levels by 47.5% over this elevated baseline, confirming robust induction of apoptosis beyond intrinsic stress signaling. This highlights the aggressive biology of pancreatic adenocarcinoma, where pro-survival and pro-death signals coexist, and underscores the therapeutic potential of overcoming inherent resistance mechanisms.

Apoptosis and autophagy are two distinct forms of cell death. Although there are obvious morphological and molecular differences between these processes, they are not completely independent (52,53). Studies have shown that apoptosis and autophagy affect and restrict each other in different cellular contexts (28-30). Increasing evidence has shown that a number of chemotherapies and anticancer drugs, such as temozolomide (in glioma), cisplatin (in gastric and ovarian cancer) and rapalogs (such aseverolimus in various solid tumors), can induce autophagy in a variety of cancer cells (54,55). Therefore, targeting of autophagy is becoming a promising strategy for cancer treatment. The unc-51 like autophagy activating kinase 1 (ULK1) complex, which includes ULK1, autophagy-related protein (ATG)13, focal adhesion kinase family-interacting protein of 200 kDa and ATG101, is a key regulator of autophagy initiation (56). The AMP-activated protein kinase (AMPK) and mTOR signaling pathways can initiate autophagy by regulating the activity of ULK1 (57). In response to nutrient or energy deprivation, AMPK activates ULK1, while mTOR inhibition promotes the formation of ULK1 complexes and initiates the autophagic process. In addition, some upstream signaling molecules such as Bcl-2 are involved in autophagosome formation by regulating the activity of Beclin 1 and affecting its binding to vacuolar protein sorting 34 (58,59). In response to autophagy signals, the C-terminal amino acid of pro-LC3 is first cleaved by ATG4, resulting in the formation of LC3I. Subsequently, ATG7 activates LC3I, which is transferred to ATG3 to be converted into LC3II, which binds to the autophagosome membrane to promote autophagy (60). In the present study, western blotting and ICC assays confirmed that SSD and GEM, both alone and in combination, increased the expression of Beclin 1 and the ratio of LC3II/LC3I in pancreatic cancer cells. MDC assays showed that the accumulation and relative fluorescence intensity of autophagic vesicles in the cytoplasm of pancreatic cancer cells were markedly increased upon combined SSD + GEM exposure compared with either treatment alone, suggesting a potential synergistic effect.

The Chou-Talalay analysis (27,61) demonstrated that low-dose SSD (4 $\mu$mol/l) synergistically enhanced GEM efficacy (CI, 0.42-0.72), which mechanistically aligns with the dual regulation of the AKT/mTOR pathway and autophagic flux. This synergistic interaction may allow dose reduction of both agents while maintaining antitumor efficacy, potentially mitigating GEM-associated toxicity in clinical settings. Particularly noteworthy is the more pronounced synergy in AsPC-1 cells (CI, 0.42-0.65 vs. 0.58-0.72 in MIA PaCa-2 cells), suggesting cell line-specific response patterns that warrant further investigation.

The therapeutic potential of this combination is further underscored by the favorable safety profile of SSD. The safety profile of SSD is supported by its selective cytotoxicity, with reported $IC_{50}$ values >20 $\mu$mol/l in normal pancreatic cells vs. 4-6 $\mu$mol/l in cancer cells (42), suggesting a favorable therapeutic window. Emerging preclinical evidence from patient-derived xenograft models has demonstrated the translational potential of TCM-derived compounds such as SSD in combination with conventional chemotherapy (19), which aligns with the present findings. Mechanistically, the observed synergy may stem from SSD's multifaceted regulation of AKT/mTOR signaling, a critical node governing both metastatic progression and cellular metabolism in pancreatic cancer (15), where concurrent pathway inhibition and autophagy induction create a synthetic lethal effect.

A recognized limitation of the present study is its focus on two pancreatic cancer cell lines without inclusion of additional *in vitro* models [such as normal cell controls or heterogeneous pancreatic ductal adenocarcinoma (PDAC) subtypes] or *in vivo* validation. These aspects are crucial to comprehensively evaluate the translational relevance and safety of the combination therapy. Therefore, future studies will prioritize expanding the biological validation to include toxicity assessments in non-malignant cells, a broader panel of cell lines representing the genetic diversity of PDAC and robust *in vivo* models to firmly establish the efficacy and therapeutic window of SSD + GEM.

In the present study, ICC staining utilizing DAB was employed to evaluate protein expression and subcellular localization. Although DAB-based methods provide advantages such as brightfield microscopy compatibility and archival stability, they are limited by poorer spatial resolution and interpretive subjectivity. To address these concerns, all ICC findings were rigorously validated through complementary quantitative approaches: Western blotting provided objective semi-quantitative measurements of protein expression, such as the Bax/Bcl-2 ratio, LC3-II/LC3-I conversion and the p-AKT/AKT ratio, and fluorescence-based assays (TUNEL, Hoechst and MDC staining) enabled high-resolution visualization of apoptosis and autophagy, corroborating ICC trends. The concordance across these orthogonal methods confirmed the reliability of the ICC data. Future studies would benefit from multiplex immunofluorescence to enhance spatial resolution for complex signaling networks.

In conclusion, the present study demonstrated that SSD inhibited proliferation, and induced autophagy and apoptosis of pancreatic cancer cells, thereby enhancing the anticancer activity of GEM. The present data further suggested that negative regulation of the AKT/mTOR signaling pathway may be, at least in part, responsible for these effects (Fig. 8). These results provide a strong rationale for the combination of GEM and SSD in the treatment of pancreatic cancer.

**Acknowledgements**

Not applicable.

**Funding**

The present study was supported by the National Natural Science Foundation of China (grant nos. 82260489 and 82560545), the Shaanxi Province Youth Talent Lifting Project (grant no. 20240316), the Shanxi Science and Technology

Department Project (grant no. 2025JC-YBQN-1175), the Innovation and Entrepreneurship Training Program for College Students (grant no. S202210719100), the General Project of Shaanxi Provincial Department of Education (grant no. 24JK0727), and Yan'an University Doctoral Research Project (grant no. YDBK2020-29).

## Availability of data and materials

The data generated in the present study may be requested from the corresponding author.

## Authors' contributions

YZ and YL conceived and designed the study, and drafted the original manuscript. RZ, YY, SZ and GL performed the experiments and analyzed the data. All authors participated in scientific discussions and data interpretation. YL contributed to data acquisition and authenticity verification. XL performed statistical analysis. YZ and YL confirm the authenticity of all the raw data. All authors have read and approved the final version of the manuscript.

## Ethics approval and consent to participate

Not applicable.

## Patient consent for publication

Not applicable.

## Competing interests

The authors declare that they have no competing interests.

## References

1. Cai J, Chen H, Lu M, Zhang Y, Lu B, You L, Zhang T, Dai M and Zhao Y: Advances in the epidemiology of pancreatic cancer: Trends, risk factors, screening, and prognosis. Cancer Lett 520: 1-11, 2021.
2. Klatte DCF, Wallace MB, Löhr M, Bruno MJ and van Leerdam ME: Hereditary pancreatic cancer. Best Pract Res Clin Gastroenterol 58-59: 101783, 2022.
3. Domagała-Haduch M, Gorzelak-Magiera A, Michalecki Ł and Gisterek-Grocholska I: Radiochemotherapy in pancreatic cancer. Curr Oncol 31: 3291-3300, 2024.
4. Brozos-Vázquez E, Toledano-Fonseca M, Costa-Fraga N, García-Ortiz MV, Díaz-Lagares Á, Rodríguez-Ariza A, Aranda E and López-López R: Pancreatic cancer biomarkers: A pathway to advance in personalized treatment selection. Cancer Treat Rev 125: 102719, 2024.
5. Miao H, Chen X and Luan Y: Small molecular gemcitabine prodrugs for cancer therapy. Curr Med Chem 27: 5562-5582, 2020.
6. Pandit B and Royzen M: Recent development of prodrugs of gemcitabine. Genes (Basel) 13: 466, 2022.
7. Cui J, Guo Y, Yin T, Gou S, Xiong J, Liang X, Lu C and Peng T: USP8 promotes gemcitabine resistance of pancreatic cancer via deubiquitinating and stabilizing Nrf2. Biomed Pharmacother 166: 115359, 2023.
8. Shu X, Zhan PP, Sun LX, Yu L, Liu J, Sun LC, Yang ZH, Ran YL and Sun YM: BCAT1 activates PI3K/AKT/mTOR pathway and contributes to the angiogenesis and tumorigenicity of gastric cancer. Front Cell Dev Biol 9: 659260, 2021.
9. Yu L, Wei J and Liu P: Attacking the PI3K/Akt/mTOR signaling pathway for targeted therapeutic treatment in human cancer. Semin Cancer Biol 85: 69-94, 2022.
10. Rahaman A, Chaudhuri A, Sarkar A, Chakraborty S, Bhattacharjee S and Mandal DP: Eucalyptol targets PI3K/Akt/mTOR pathway to inhibit skin cancer metastasis. Carcinogenesis 43: 571-583, 2022.
11. Zhou X, Zhao J, Yan T, Ye D, Wang Y, Zhou B, Liu D, Wang X, Zheng W, Zheng B *et al*: ANXA9 facilitates S100A4 and promotes breast cancer progression through modulating STAT3 pathway. Cell Death Dis 15: 260, 2024.
12. Jiang Q, Guan Y, Zheng J and Lu H: TBK1 promotes thyroid cancer progress by activating the PI3K/Akt/mTOR signaling pathway. Immun Inflamm Dis 11: e796, 2023.
13. Wang S, Cheng Z, Cui Y, Xu S, Luan Q, Jing S, Du B, Li X and Li Y: PTPRH promotes the progression of non-small cell lung cancer via glycolysis mediated by the PI3K/AKT/mTOR signaling pathway. J Transl Med 21: 819, 2023.
14. Wang S, Zhang C, Xu Z, Chen MH, Yu H, Wang L and Liu R: Differential impact of PI3K/AKT/mTOR signaling on tumor initiation and progression in animal models of prostate cancer. Prostate 83: 97-108, 2023.
15. Mortazavi M, Moosavi F, Martini M, Giovannetti E and Firuzi O: Prospects of targeting PI3K/AKT/mTOR pathway in pancreatic cancer. Crit Rev Oncol Hematol 176: 103749, 2022.
16. Huang L, Sun J, Ma Y, Chen H, Tian C and Dong M: MSI2 regulates NLK-mediated EMT and PI3K/AKT/mTOR pathway to promote pancreatic cancer progression. Cancer Cell Int 24: 273, 2024.
17. Shimia M, Amini M, Ravari AO, Tabnak P, Valizadeh A, Ghaheri M and Yousefi B: Thymoquinone reversed doxorubicin resistance in U87 glioblastoma cells via targeting PI3K/Akt/mTOR signaling. Chem Biol Drug Des 104: e14587, 2024.
18. Wang M, Xue W, Yuan H, Wang Z and Yu L: Nano-drug delivery systems targeting CAFs: A promising treatment for pancreatic cancer. Int J Nanomedicine 19: 2823-2849, 2024.
19. Zhang Y, Xu H, Li Y, Sun Y and Peng X: Advances in the treatment of pancreatic cancer with traditional Chinese medicine. Front Pharmacol 14: 1089245, 2023.
20. Manoharan S, Deivendran B and Perumal E: Chemotherapeutic potential of saikosaponin D: Experimental evidence. J Xenobiot 12: 378-405, 2022.
21. Liu G, Guan Y, Liu Y, Wang Y, Zhang J, Liu Y and Liu X: Saikosaponin D inducing apoptosis and autophagy through the activation of endoplasmic reticulum stress in glioblastoma. Biomed Res Int 2022: 5489553, 2022.
22. Tang JC, Long F, Zhao J, Hang J, Ren YG, Chen JY and Mu B: The effects and mechanisms by which saikosaponin-D enhances the sensitivity of human non-small cell lung cancer cells to gefitinib. J Cancer 10: 6666-6672, 2019.
23. Hu J, Li P, Shi B and Tie J: Effects and mechanisms of saikosaponin d improving the sensitivity of human gastric cancer cells to cisplatin. ACS Omega 6: 18745-18755, 2021.
24. Zhang CY, Jiang ZM, Ma XF, Li Y, Liu XZ, Li LL, Wu WH and Wang T: Saikosaponin-d inhibits the hepatoma cells and enhances chemosensitivity through SENP5-dependent inhibition of gli1 sumoylation under hypoxia. Front Pharmacol 10: 1039, 2019.
25. Liang J, Sun J, Liu A, Chen L, Ma X, Liu X and Zhang C: Saikosaponin D improves chemosensitivity of glioblastoma by reducing the its stemness maintenance. Biochem Biophys Rep 32: 101342, 2022.
26. Tang TT, Jiang L, Zhong Q, Ni ZJ, Thakur K, Khan MR and Wei ZJ: Saikosaponin D exerts cytotoxicity on human endometrial cancer ishikawa cells by inducing apoptosis and inhibiting metastasis through MAPK pathways. Food Chem Toxicol 177: 113815, 2023.
27. Chou TC: Drug combination studies and their synergy quantification using the Chou-Talalay method. Cancer Res 70: 440-446, 2010.
28. Xi H, Wang S, Wang B, Hong X, Liu X, Li M, Shen R and Dong Q: The role of interaction between autophagy and apoptosis in tumorigenesis (Review). Oncol Rep 48: 208, 2022.
29. Sorice M: Crosstalk of autophagy and apoptosis. Cells 11: 1479, 2022.
30. Liu S, Yao S, Yang H, Liu S and Wang Y: Autophagy: Regulator of cell death. Cell Death Dis 14: 648, 2023.
31. Niu X, You Q, Hou K, Tian Y, Wei P, Zhu Y, Gao B, Ashrafizadeh M, Aref AR, Kalbasi A, *et al*: Autophagy in cancer development, immune evasion, and drug resistance. Drug Resist Updat 78: 101170, 2025.
32. Liu J, Wu Y, Meng S, Xu P, Li S, Li Y, Hu X, Ouyang L and Wang G: Selective autophagy in cancer: mechanisms, therapeutic implications, and future perspectives. Mol Cancer 23: 22, 2024.

33. Zhao Y, Tang J, Jiang K, Liu SY, Aicher A and Heeschen C: Liquid biopsy in pancreatic cancer-current perspective and future outlook. Biochim Biophys Acta Rev Cancer 1878: 188868, 2023.
34. Zhong BH, Ma YT, Sun J, Tang JT and Dong M: Transcription factor FOXF2 promotes the development and progression of pancreatic cancer by targeting MSI2. Oncol Rep 52: 93, 2024.
35. Chen J, Hua Q, Wang H, Zhang D, Zhao L, Yu D, Pi G, Zhang T and Lin Z: Meta-analysis and indirect treatment comparison of modified FOLFIRINOX and gemcitabine plus nab-paclitaxel as first-line chemotherapy in advanced pancreatic cancer. BMC Cancer 21: 853, 2021.
36. Ji J, Wen Q, Yu Y, Xiong F, Zheng X and Ruan S: Personalized traditional Chinese medicine in oncology: Bridging the macro state with micro targets. Am J Chin Med 14: 1-34, 2025.
37. Ke Y, Pan Y, Huang X, Bai X, Liu X, Zhang M, Wei Y, Jiang T and Zhang G: Efficacy and safety of traditional Chinese medicine (TCM) combined with immune checkpoint inhibitors (ICIs) for the treatment of cancer: a systematic review and meta-analysis. Front Pharmacol 31: 1661503, 2025.
38. Okuno K, Xu C, Pascual-Sabater S, Tokunaga M, Han H, Fillat C, Kinugas Y and Goel A: Berberine overcomes gemcitabine-associated chemoresistance through regulation of Rap1/PI3K-Akt signaling in pancreatic ductal adenocarcinoma. Pharmaceuticals (Basel) 15: 1199, 2022.
39. Bhattacharyya S, Ghosh H, Covarrubias-Zambrano O, Jain K, Swamy KV, Kasi A, Hamza A, Anant S, Van Saun M, Weir SJ, *et al*: Anticancer activity of novel difluorinated curcumin analog and its inclusion complex with 2-hydroxypropyl-β-cyclodextrin against pancreatic cancer. Int J Mol Sci 24: 6336, 2023.
40. Ashour ML and Wink M: Genus bupleurum: A review of its phytochemistry, pharmacology and modes of action. J Pharm Pharmacol 63: 305-321, 2011.
41. Cheng Y, Liu G, Li Z, Zhou Y and Gao N: Screening saikosaponin d (SSd)-producing endophytic fungi from Bupleurum scorzonerifolium Willd. World J Microbiol Biotechnol 38: 242, 2022.
42. Lai M, Ge Y, Chen M, Sun S, Chen J and Cheng R: Saikosaponin D inhibits proliferation and promotes apoptosis through activation of MKK4-JNK signaling pathway in pancreatic cancer cells. Onco Targets Ther 13: 9465-9479, 2020.
43. Conroy T, Castan F, Lopez A, Turpin A, Ben Abdelghani M, Wei AC, Mitry E, Biagi JJ, Evesque L, Artru P *et al*: Five-year outcomes of FOLFIRINOX vs. gemcitabine as adjuvant therapy for pancreatic cancer: A randomized clinical trial. JAMA Oncol 8: 1571-1578, 2022.
44. Sun EJ, Wankell M, Palamuthusingam P, McFarlane C and Hebbard L: Targeting the PI3K/Akt/mTOR pathway in hepatocellular carcinoma. Biomedicines 9: 1639, 2021.
45. Kale J, Kutuk O, Brito GC, Andrews TS, Leber B, Letai A and Andrews DW: Phosphorylation switches Bax from promoting to inhibiting apoptosis thereby increasing drug resistance. EMBO Rep 19: e45235, 2018.
46. Li X, He S and Ma B: Autophagy and autophagy-related proteins in cancer. Mol Cancer 19: 12, 2020.
47. Mehra S, Deshpande N and Nagathihalli N: Targeting PI3K pathway in pancreatic ductal adenocarcinoma: Rationale and progress. Cancers (Basel) 13: 4434, 2021.
48. Sheng W, Shi X, Lin Y, Tang J, Jia C, Cao R, Sun J, Wang G, Zhou L and Dong M: Musashi2 promotes EGF-induced EMT in pancreatic cancer via ZEB1-ERK/MAPK signaling. J Exp Clin Cancer Res 39: 16, 2020.
49. Johnson DE, O'Keefe RA and Grandis JR: Targeting the IL-6/JAK/STAT3 signalling axis in cancer. Nat Rev Clin Oncol 15: 234-248, 2018.
50. Deer EL, González-Hernández J, Coursen JD, Shea JE, Ngatia J, Scaife CL, Firpo MA and Mulvihill SJ: Phenotype and genotype of pancreatic cancer cell lines. Pancreas 39: 425-435, 2010.
51. Fianco G, Mongiardi MP, Levi A, De Luca T, Desideri M, Trisciuoglio D, Del Bufalo D, Cinà I, Di Benedetto A, Mottolese M, *et al*: Caspase-8 contributes to angiogenesis and chemotherapy resistance in glioblastoma. Elife 6: e22593, 2017.
52. Wei S, Han C, Mo S, Huang H and Luo X: Advancements in programmed cell death research in antitumor therapy: A comprehensive overview. Apoptosis 30: 401-421, 2025.
53. Das S, Shukla N, Singh SS, Kushwaha S, Shrivastava R: Mechanism of interaction between autophagy and apoptosis in cancer. Apoptosis 26: 512-533, 2021.
54. Hajdú B, Holczer M, Horváth G, Szederkényi G and Kapuy O: Fine-tuning of mTORC1-ULK1-PP2A regulatory triangle is crucial for robust autophagic response upon cellular stress. Biomolecules 12: 1587, 2022
55. Fujiwara N, Usui T and Nagai H: Regulation of the Beclin 1/VPS34 complex by post-translational modifications. Biochem Biophys Res Commun 566: 155-161, 2021.
56. Pareek G and Kundu M: Physiological functions of ULK1/2. J Mol Biol 436: 168472, 2024.
57. Lu G, Wu Z, Shang J, Xie Z, Chen C and Zhang C: The effects of metformin on autophagy. Biomed Pharmacother 137: 111286, 2021.
58. Fujiwara N, Shibutani S, Ohama T and Sato K: Protein phosphatase 6 dissociates the beclin 1/Vps34 complex and inhibits autophagy. Biochem Biophys Res Commun 552: 191-195, 2021.
59. Bekker M, Abrahams S, Loos B and Bardien S: Can the interplay between autophagy and apoptosis be targeted as a novel therapy for Parkinson's disease? Neurobiol Aging 100: 91-105, 2021.
60. Vujić N, Bradić I, Goeritzer M, Kuentzel KB, Rainer S, Kratky D and Radović B: ATG7 is dispensable for LC3-PE conjugation in thioglycolate-elicited mouse peritoneal macrophages. Autophagy 17: 3402-3407, 2021.
61. Foucquier J and Guedj M: Analysis of drug combinations: Current methodological landscape. Pharmacol Res Perspect 3: e00149, 2015.